

Merging of a massive black hole binary II

C. Zier^{1*}

¹*Raman Research Institute, Bangalore 560080, India*

Accepted Received

ABSTRACT

In this paper, the second in a series of two, we justify two important assumptions on which the result is based that in course of a galaxy merger the slingshot ejection of bound stars is sufficiently efficient to allow a supermassive black hole binary to merge. A steep cusp with a power law index of 2.5–3 is required which is as massive as the binary and surrounds the BHs when the binary becomes hard. This cusp is probably formed when both clusters, surrounding each black hole, merge and combine with the matter funneled into the center. We find this profile to be in agreement with observed post-merger distributions after the cusp has been destroyed. The time dependency we derive for the merger predicts that stalled black holes, if they exist at all, will preferably be found in less than ~ 0.2 pc distance. To test this prediction we compute the current semimajor axis of 12 candidates of ongoing mergers. We find all binaries unambiguously to be already in the last phase when they decay due to the emission of gravitational waves. Therefore, in striking contradiction with predictions of a depleted loss-cone, the absence of even a single source in the slingshot phase strongly supports our previous and current results: Binaries merge due to slingshot ejection of stars which have been funneled into the central regions in course of a galaxy collision.

Key words: black hole physics – galaxies: evolution – galaxies: interaction – galaxies: kinematics and dynamics

1 INTRODUCTION

The formation of a supermassive black hole binary (BHB) is the natural consequence of two widely accepted assumptions: Galaxies harbour a supermassive black hole (BH) in their center and galaxies merge with each other. Such BHBs, merged and not yet merged, are important because they are used to explain a wide variety of features observed in galaxies. For a detailed review on observational evidence of BHBs see Komossa (2003) or an updated version, Komossa (2006). The evolution of the merging BHs can be subdivided into three successive phases (Begelman et al. 1980): In the beginning both cores spiral inwards to their common center due to dynamical friction. Once the BHs bind to each other on the parsec scale and form a hard binary they keep on merging due to slingshot ejection of stars. Finally, in the third phase, the binary continues to decay owing to the emission of gravitational waves. While the first and third phase are well investigated it is still a matter of debate whether the slingshot ejection of stars in the second phase is efficient enough to enable the binary to enter the final phase or whether the merging process comes to a halt due to loss-cone depletion. Even though numerical scattering experiments showed that the BHs merge on scales of

10^{8-9} yr (Quinlan 1996; Makino 1997; Quinlan & Hernquist 1997; Milosavljević & Merritt 2001; Zier & Biermann 2001) it is argued in all publications but the last that the loss-cone becomes depleted long before the binary enters the third phase and the binary probably gets stalled. This reasoning is based on the assumption that the binary is embedded in a flat spherically symmetric core which is derived from the central density profiles of elliptical galaxies (Berczik et al. 2005). According to hierarchical models for galaxy formation this type of galaxy has experienced a major merger previously and therefore its mass has been redistributed from the central parts to the outer regions, resulting in a flat profile after the merger.

While there is no conclusive observational evidence for stalled binaries various sources suggest a generally successful merger of the BHs. Haehnelt & Kauffmann (2002) argued that if the merging time would exceed a Hubble time the binary should become ejected in about 40% of bright ellipticals when merging with a third galaxy. They pointed out that this would be in contradiction with the BHs which have been observed indirectly in all nearby elliptical galaxies and with the small scatter of the $M_{\text{BH}} - \sigma_*$ relation (e.g. Gebhardt et al. 2000; Tremaine et al. 2002). A certain class of sources, the so-called X-shaped radio galaxies (XRGs), can be well explained in terms of a completed merger of a BHB, an interpretation first

* E-mail: chzier@mpifr-bonn.mpg.de

used by Rottmann (2001). When the BHs finally coalesce the spin axis is rapidly realigned into the direction of the orbital angular momentum so that the old and new lobes appear as an X on the sky (Zier & Biermann 2001; Dennett-Thorpe et al. 2002; Zier & Biermann 2002; Gergely & Biermann 2007). During the third phase the rapidly precessing jet produces effectively a powerful wind, which entrains the environmental gas and is identified by Gergely & Biermann (2007) with a superdisc, discussed by Gopal-Krishna, et al. (2007). A merger is also held responsible for Z-shaped radio galaxies, where the secondary galaxy bends the jet of the primary into a Z-shape before the BHs coalesce (Gopal-Krishna, et al. 2003; Zier 2005), for double-double radio galaxies (Schoenmakers et al. 2000; Liu et al. 2003) and possibly for compact symmetric objects (Zier & Biermann 2002). Recently the sample of known XRGs has been increased considerably by Cheung (2007). This can be used for systematic studies and hence might support the merging scenario as formation mechanism of XRGs. Other sources suggest that the BHs have not yet merged and are still orbiting around each other. Helical jet patterns could be explained in this way (Begelman et al. 1980) as well as semi-periodic changes in lightcurves (e.g. Sillanpää et al. 1988; Katz 1997). However, this does not necessarily mean that the BHs are stalled, the binary might still decay.

In a recent letter (Zier 2006, from now on Paper I) we showed that the slingshot ejection of stars in the second phase is efficient enough to allow the BHs to shrink to the third phase and coalesce within less than a Hubble time. Unlike in previous numerical simulations where the focus was on stars scattered off the binary, we focused on the stars bound in the potential of the BHs. The results showed that if the binary by the time it becomes hard is surrounded by a flat cusp with a power law index $\gamma \lesssim 2$, as it appears *after* the merger and has been used in previous simulations, it will stall in this phase unless the cusp is very massive. However, we predict that the cusp is as massive as the binary and sufficiently steep ($\gamma \gtrsim 2.5$) *during* the merger when the binary becomes hard. The ejection of this mass out of the potential of the BHs extracts enough energy so that the binary can enter the third phase and the BHs coalesce. We argued that such a profile is formed during the merger. Parameters like the initial mass and velocity distributions in the isolated galaxies as well as the magnitude and orientation of both galactic spins and the orbital angular momentum relative to each other have a strong influence on the merger and the morphology of the remnant (Toomre & Toomre 1972). While the galaxies are merging energy is dissipated and angular momentum redistributed with some fractions compensating each other. Large amounts of mass move on highly eccentric orbits (Rauch & Tremaine 1996) in a potential that is strongly non-spherically symmetric. Low angular momentum matter accumulates in the center. Together with both cores which surround each BH and whose density increases considerably during the merger (Barnes & Hernquist 1996) this matter forms a massive and steep cusp by the time the binary becomes hard. This cusp is only transient because it will be destroyed by the merging binary and therefore is not likely to be observed. However, this should be the appropriate profile in order to simulate the second phase.

In the present article, after repeating in Section 2 the

results from Paper I which we will need in this paper, we will justify in more detail our assumptions for the kick-parameter k (Section 3) and the neglect of the cluster potential (Section 4). Afterwards we show that the fraction of mass which is required to become ejected is in agreement with the total mass of the galaxy. We also show that the profile which at the beginning of the second phase is required to allow the BHs to coalesce is in agreement with the observed post-merger profiles after the binary has destroyed the cusp (Section 5). In Section 6 we briefly consider the evolution of a merger in time before we compare the effects of multiple mergers on the ejected mass with numerical simulations in Section 7. Afterwards we examine observational evidence for ongoing mergers which might have become stalled (Section 8) and finally summarize our results in Section 9.

2 PRELIMINARIES

First we repeat the basic assumptions and some results from Paper I which we will use in the present article. It is assumed that the BHs, moving on Keplerian orbits, have formed a hard binary and that the origin coincides with the center of mass. We define the mass ratio $q \equiv m_2/m_1 \leq 1$. The total and reduced mass are $M_{12} = m_1 + m_2$ and $\mu = m_1 m_2 / M_{12}$, respectively. Hence, the energy of the binary is

$$E_{\text{bin}} = -\frac{GM_{12}\mu}{2a} \quad (1)$$

and the relative velocity between the BHs is

$$v_{\mu} = \sqrt{\frac{GM_{12}}{a}}, \quad (2)$$

where a is the semimajor axis of the binary. If the cluster mass M_c is distributed according to the power law $\rho = \rho_0(r/r_0)^{-\gamma}$ between the radii r_i and r_c with

$$\rho_0 = \frac{M_c}{4\pi r_0^3} \begin{cases} \frac{3-\gamma}{(r_c/r_0)^{3-\gamma} - (r_i/r_0)^{3-\gamma}}, & \gamma \neq 3 \\ \frac{1}{\ln(r_c/r_i)}, & \gamma = 3. \end{cases} \quad (3)$$

we obtain for the mass within r

$$M(r) = M_c \begin{cases} \frac{r^{3-\gamma} - r_i^{3-\gamma}}{r_c^{3-\gamma} - r_i^{3-\gamma}}, & \gamma \neq 3 \\ \frac{\ln(r/r_i)}{\ln(r_c/r_i)}, & \gamma = 3. \end{cases} \quad (4)$$

Note that in the following we will refer to the logarithmic slopes of density profiles, $d \log \rho / d \log r$, simply as slopes. In Paper I, we showed that a mass of about $2M_{12}$ is bound to the binary, of which a large fraction is expected to be in the loss-cone. For stars belonging to this population, the initial energy in the potential of the binary is

$$E_{*,i} = -(1-\epsilon) \frac{GM_{12}m_*}{2r_-}, \quad (5)$$

where $\epsilon < 1$ is the eccentricity of the star's orbit and r_- the pericenter. We approximated the potential of the binary to first order with a point potential of mass M_{12} located at the center of the cluster. This introduces only minor deviations with a maximum of a factor of less than 2 for $q = 1$. In Section 4, we will show that it is justified to neglect the potential of the cluster itself when computing the binding

energy of the stars in Eq. (5). After its ejection the formerly bound star will have a positive energy which we can scale with the factor κ to its initial energy for circular orbits ($\epsilon = 0$):

$$E_{*,f} = \kappa \frac{GM_{12}m_*}{2r_-}. \quad (6)$$

According to Quinlan (1996) the dominant contribution to the hardening of the binary comes from stars whose pericenter is about the semimajor axis of the binary, independent of the density profile. Hence replacing r_- with a we obtain for the energy change $E_{*,f} - E_{*,i}$ of the star:

$$\Delta E_* = (1 - \epsilon + \kappa) \frac{GM_{12}m_*}{2a} \equiv k \frac{GM_{12}m_*}{2a} = k \frac{m_* v_\mu^2}{2}. \quad (7)$$

Note that for pericenters smaller than a the initial energy of the star would be smaller and therefore the energy change larger, resulting in an increased kick-parameter k .

In the limit $m_* \ll m_2$ we can replace m_* with dm and write Eq. (7) in its infinitesimal form. Equating it with the change of the binary's energy in Eq. (1) due to the ejection of the mass dm yields the differential equation

$$\frac{da}{a} = -k \frac{dm}{\mu}, \quad (8)$$

which relates the shrinking of the binary to the amount of the ejected mass. Integrating Eq. (8) from a_g to a_h we showed in Paper I that the binary has to eject the mass

$$m_{\text{ej}} = \frac{\mu}{k} \ln \frac{a_h}{a_g}. \quad (9)$$

The semimajor axis where the binary becomes hard, a_h , and where emission of gravitational waves starts to dominate the decay, a_g , mark the transitions from phase 1 to 2 and phase 2 to 3, respectively. While a_g is well defined (see Eq. (75)), there is no unique prescription for the semimajor axis where the binary becomes hard. However, the ratio of these distances $\eta \equiv a_h/a_g$ is agreed to range from about 20 to 100, see the discussion in Paper I and references therein. In the following we assume that the binary is hard and do not worry about the exact value of a_h . We showed that the ejection of about m_{ej} is sufficient for the binary to shrink from a_h to a_g , provided this mass is distributed according to a steep power law with an index $\gamma \gtrsim 2.5$. Therefore, we concluded, the coalescence of the BHs is very likely in the course of a galaxy merger where a large amount of mass with low angular momentum is accumulated in the central region.

3 THE KICK-PARAMETER k

One of our basic assumptions in Paper I is a kick-parameter $k = 1$. In the literature we can find various prescriptions for k which we defined in Eq. (7). If we express the final energy of the ejected star in terms of its velocity at infinity, $E_{*,f} = m_* v_\infty^2/2$ we can write $\kappa = (v_\infty/v_\mu)^2$, where we made use of Eqs. (6) and (2) and replaced the pericenter of the orbit of the star with the semimajor axis of the binary. This form can be used in the relation between the scaling parameters obtained from Eq. (7), $k = 1 - \epsilon + \kappa$. From scattering experiments Quinlan (1996) finds that most of the stars are ejected with a final velocity $v_\infty \approx (3/2)v_\mu \sqrt{m_2/M_{12}} =$

$(3/2)v_\mu \sqrt{q/(1+q)}$ and hence we obtain

$$k = 1 - \epsilon + \frac{9}{4} \frac{q}{1+q}. \quad (10)$$

Quinlan argued that the energy gained by a star can basically be attributed to the interaction with the smaller BH in the limit $m_1 \gg m_2$, because the larger BH acts as a fixed potential. He then derives an expression for the energy change which is proportional to $m_2/M_{12} = q/(1+q)$. However, because m_1 and m_2 are bound to each other also the acting forces correspond to each other so that the larger mass m_1 compensates for the smaller semimajor axis of its orbit. Therefore it does not seem to be justified to approximate it as a fixed point potential compared to the potential generated by m_2 . The potential of the BHs is $\Phi_i = Gm_i/r_i$. As they move along their orbits a test mass m_* , which is fixed in space, experiences a change in the potential which is proportional to the displacement of the BHs:

$$d\Phi_i = \frac{Gm_i}{r_i^2} dr_i. \quad (11)$$

We assume that the displacement dr_i of the mass m_i corresponds to the semimajor axis of its orbit a_i . Expressing this in terms of the semimajor axis of the binary a , i.e. $a_1 = aq/(1+q)$ and $a_2 = a/(1+q)$, we can write

$$d\Phi_1 = \frac{Gm_1}{r_1^2} a \frac{q}{1+q}, \quad d\Phi_2 = \frac{Gm_2}{r_2^2} a \frac{1}{1+q}. \quad (12)$$

The binary shrinks mostly due to the interaction with stars whose closest approach corresponds to the semimajor axis (Quinlan 1996). Hence we can replace r_1 and r_2 with a , resulting in equal changes of both potentials, $\Delta\Phi = (Gm_1/a)q/(1+q) = v_\mu^2 \mu/M_{12}$. If the star was moving on a parabolic orbit and this energy is transferred from both BHs to the star its final velocity is $v_\infty = v_\mu \sqrt{2\mu/M_{12}}$ so that

$$\kappa = 2 \frac{\mu}{M_{12}} = 2 \frac{q}{(1+q)^2}. \quad (13)$$

This result has been cited before to have been obtained by Saslaw et al. (1974) in numerical experiments. Apart from a factor $1/(1+q)$, which has a minimum of $1/2$ for $q = 1$, this result is very similar to that obtained by Quinlan above. Similar values have also been found before. In simulations of close encounters of stars with a hard equal-mass binary of zero eccentricity, Hills & Fullerton (1980) obtained for the mean velocity of stars at infinity $v_\infty \approx 0.84 v_\mu$, and hence $\kappa \approx 0.71$. Later Roos (1981) performed numerical computations with a varying mass ratio and approximated the kick-parameter with $k = 2\mu/M_{12}$, the same result we have found above for κ . For parabolic orbits, as we have assumed above, these parameters are equal and our crude estimate is in good agreement with his result.

More recently Zier (2000) simulated a stellar cluster bound in the potential of a BHB which is moving on fixed circular orbits. He carried out several runs for different mass ratios ($q = 0.01, 0.1$ and 1) and various initial density profiles of the stars (Gaussian or power laws with index $\gamma = 2$ or 4). For every run we binned the initial eccentricities of the orbits and computed the kick-parameter for each bin. In Fig. 1, we show the thus obtained k in dependency on the eccentricity and find a distinct linear correlation. We can not detect a clear dependency on the kind of the initial profile in the plot. However, the data show a weak positive

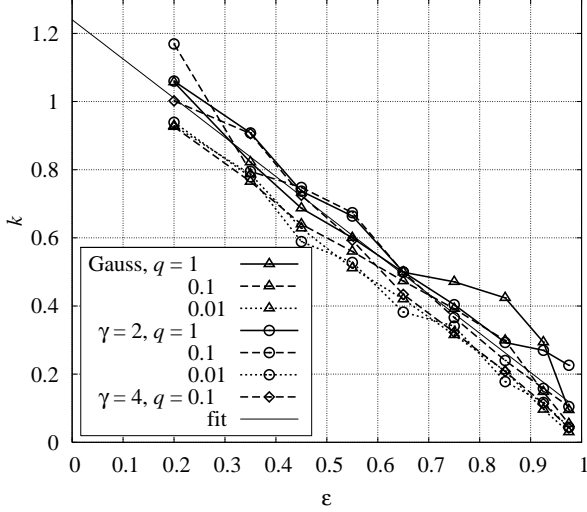


Figure 1. Data show that the kick-parameter is roughly a linear function of the eccentricity of the stellar orbit. While k tends to increase with q it does not seem to depend on the choice of the initial profile. The fit is drawn by eye using all data points.

dependency of k on the mass ratio q . This is in agreement with the previous results given above in Eqs. (10) and (13) if we write $k = 1 - \epsilon + \kappa$, although the dependency on q exhibited in the data is weaker. However, we find that $k \approx 1$ is a good approximation for $\epsilon \lesssim 0.4$. Note that the simulations by Zier (2000) did not take into account the potential of the stellar cluster and hence the real values for k should actually be larger than those displayed in Fig. 1, see next Section. Because Eq. (10) is less steep than the data in Fig. 1 it suggests this equation generally yields slightly larger values for the kick-parameter if the mass ratio is not too small.

Comparing our definition of the kick-parameter with that of Yu (2002) for K we find $k = 2Kq/(1+q)^2$. Making use of the results of Quinlan (1996), Yu obtains $K \approx 1.6$. This translates to a maximum value of $k = 0.8$ for $q = 1$, roughly in agreement with the previous results. Note that in Paper I we did not include the factor $\mu/M_{12} = q/(1+q)^2$ and so derived a too large value of $k = 3.2$. Because we just quoted this result and used $k = 1$ throughout the paper none of the results and conclusions obtained there are affected.

In Eq. (7) we defined k after having replaced the pericenter of the star r_- with the semimajor axis a of the binary. Because only stars with $r_- \lesssim a$ can interact with the binary and become ejected and a pericenter less than a would increase the kick-parameter (keeping the eccentricity constant) the values we derived should actually be a lower limit. In conclusion we can say that the above results clearly show that k is of order of 1 unless the stars are moving on very eccentric orbits (keeping $r_- = a$ constant, i.e. stars are only weakly bound, what is very unlikely due to dissipation of energy during the merger) and the mass ratio is very small. Therefore our choice of $k = 1$ in Paper I was well justified and we continue to use this value in the present paper.

3.1 The influence of the cluster potential on k

After a star interacted with the binary it will be ejected from the potential of the BHs. This might not happen after the first interaction, but ultimately it will be ejected unless before the next encounter with the binary the pericenter is shifted due to star-star interactions to distances too large as to interact with the binary. Or the binary has shrunk in the meantime to a semimajor axis much smaller than the pericenter of the star, again resulting in no more interactions. However, this will happen most likely only in the beginning of the merger when the evolution is fastest (see Section 6) to stars whose energy is close to zero after the last interaction so that they have been almost ejected anyway.

Interacting with the binary some stars will be accelerated to a speed which exceeds the escape velocity of the binary, but is less than the escape velocity of the combined potentials of the BHs and the cluster. These stars stay bound to the center. After multiple interactions with the binary the fraction of stars whose pericenters have become larger relative to the semimajor axis of the binary for the reasons given above will remain bound in the cluster without interacting with the binary anymore. On longer time scales they might diffuse back into the loss-cone. The other fraction eventually becomes ejected from the total potential of the BHs and cluster after multiple encounters. Hence this delayed ejected fraction, emerging because of the inclusion of the cluster potential, increases the kick-parameter on average. At radii $r \geq r_c$ the star's specific energy is

$$\begin{aligned} \mathcal{E}_* &= \frac{v^2}{2} - \frac{G(M_{12} + M_c)}{r} \\ &= \frac{v^2}{2} - \frac{GM_{12}}{r}(1+f), \end{aligned} \quad (14)$$

where $f \equiv M_c/M_{12}$, with $f > 1$. The escape velocity in the combined potential at $r > r_c$ is $v_{\text{esc}}^2 = 2(1+f)GM_{12}/r$ and for the velocity of the star in the potential of the binary only we can write $v^2(r) = 2(\mathcal{E}_* + GM_{12}/r)$. If we require that this velocity is at least as large as the escape velocity at $r = r_c$ we obtain for the specific energy the relation $\mathcal{E}_* \geq fGM_{12}/r_c$. Using this again in the expression for the star's velocity in the limit of an infinite radius yields $v_\infty^2 = 2\mathcal{E}_* \geq 2fv_\mu^2 a/r_c$. Therefore the condition that the stars become ejected from the combined potential of the binary and cluster can be written as

$$\kappa \geq 2f \frac{a}{r_c}. \quad (15)$$

κ is determined using only the binary potential. For a star which eventually escapes from the binary and the cluster this parameter is increasing with the normalized cluster mass f . In comparison with a neglected cluster potential ($f = 0$) Eq. (15) shows that including this potential increases κ . This results in a larger kick-parameter of the delayed ejected fraction and therefore also of the mean value of k of all ejected stars. On the other hand we can use Eq. (15) to derive a maximum cluster mass for which stars will be ejected,

$$f \leq \frac{r_c}{a} \frac{\kappa}{2} = \frac{r_c}{a} \frac{k + \epsilon - 1}{2}. \quad (16)$$

With our results from the previous Section and assuming that $r_c \gg a$ this relation still allows the cluster mass to exceed the binary's mass by a factor of a few, as required by a successful merger. Therefore most of the stars get a kick

large enough to escape from the center, even if we neglect the cluster potential. Consequently the fraction of delayed ejected stars is small, only slightly increasing the mean of k . This is in agreement with Yu (2002) who finds that especially for $a \ll a_h$ stars generally escape from the binary and cluster. We can summarize that including the cluster potential tends to increase on average the value of the parameter k so that the values obtained above are rather lower limits.

4 THE CLUSTER POTENTIAL

We also have to check whether it is justified to neglect the cluster potential when computing the potential energy of stars bound by the binary, our second basic assumption in Paper I. If initially stars in the cluster are not bound by the BHs, they are at least bound by the cluster itself. The energy of a star before and after the interaction with the BHs is

$$E_{*,i} = \frac{m}{2}v_i^2 - m(\Phi_{\text{bin}} + \Phi_c) \quad (17)$$

$$E_{*,f} = \frac{m}{2}v_f^2 - m(\Phi_{\text{bin}} + \Phi_c), \quad (18)$$

with Φ_c and Φ_{bin} being the potential of the cluster and the binary, respectively. If we compare the initial and final energy of the star at the same radius and assume that both potentials did not change during the time of the interaction between the binary and the star we can write for the change of the energy

$$\Delta E_* = E_{*,f} - E_{*,i} = \frac{m}{2}(v_f^2 - v_i^2).$$

Taking the circular velocity in a point potential as the typical velocity of a star in the cluster we showed in Paper I that a mass of about $2M_{12}$ is gravitationally bound to the binary. Depending on the power law index of the mass distribution the radius of a sphere which contains twice the mass of the binary is (Eq. (4))

$$r_b = r_i \begin{cases} \left(1 + 2\frac{M_{12}}{M_c} \left[\left(\frac{r_c}{r_i}\right)^{3-\gamma} - 1\right]\right)^{1/(3-\gamma)}, & \gamma \neq 3 \\ \left(\frac{r_c}{r_i}\right)^{2M_{12}/M_c}, & \gamma = 3. \end{cases} \quad (19)$$

For a valid solution of course the relation $M_c > 2M_{12}$ must be satisfied. In this range the radius r_b is increasing with decreasing γ , i.e. larger for flatter profiles. For $\gamma = 2$ and $r_i \ll r_c$ we have $r_b = 2r_c M_{12}/M_c$, independent of r_i . If the cluster is four times as massive as the binary and we assume $r_c \approx 100$ pc we obtain for r_b about 50 pc, i.e. a radius much larger than the semimajor axis a_h where the binary becomes hard. For $\gamma = 3$ and $M_c = 4M_{12}$ we find $r_b = \sqrt{r_i r_c}$, i.e. the geometrical mean. With $r_i = 0.01$ and $r_c = 100$ pc this is 1 pc. Thus a mass of $2M_{12}$ is contained in the central cusp and bound to the binary when it becomes hard.

In Paper I we assumed the star to be bound to the binary, i.e. $E_{*,i}$ is negative even if Φ_c is neglected in Eq. (17). Then v_i is less than the escape velocity from the binary what is roughly true for stars within the sphere of radius $\sim r_b$. It is this bound population on which we focused in our previous paper and which we also consider in the present work. When we calculated the energy of the stars and derived the mass

which is required to be ejected in order to extract sufficient energy so that the BHs merge, we neglected the potential of the cluster. This we will justify here by comparing the energy of a star in the potential of the binary with its energy in the potential of a stellar cluster whose mass is distributed according to a power law with index 2 or 3.

In case of $\rho = \rho_0(r/r_0)^{-2}$ we can write Poisson's equation as

$$\nabla^2 \Phi_c = 4\pi G \rho = s/r^2, \quad (20)$$

where we have introduced the constant $s \equiv 4\pi G \rho_0^2$. The stars in the cluster are distributed between r_i and r_c , the inner and the cluster radius, respectively. With M_c being the total mass of the cluster we can write $s = GM_c/(r_c - r_i)$. Integrating Eq. (20) twice we obtain for the potential in the range $r_i < r < r_c$

$$\Phi_c(r) = \Phi_c(r_i) + s \left(\ln \frac{r}{r_i} + \frac{r_i}{r} - 1 \right) - r_i^2 \left. \frac{\partial \Phi}{\partial r} \right|_{r_i} \left(\frac{1}{r} - \frac{1}{r_i} \right). \quad (21)$$

Because the mass is spherically symmetric distributed and there is no mass within r_i , no force is acting on a particle in this range. Therefore $F = -\partial\Phi/\partial r$ has to vanish at $r = r_i$. On the other hand the force acting on a particle outside the cluster is the same as that of a pointmass M_c located at the origin, $-GM_c/r^2$ (Newton's second theorem). Evaluating this condition at $r = r_c$ we can write the potential in the form

$$\Phi_c(r) = -GM_c \begin{cases} \frac{1}{r_c - r_i} \ln \frac{r_c}{r_i}, & 0 \leq r \leq r_i \\ \frac{1}{r_c - r_i} \left(1 - \frac{r_i}{r} + \ln \frac{r_c}{r}\right), & r_i \leq r \leq r_c \\ \frac{1}{r}, & r_c \leq r. \end{cases} \quad (22)$$

The potential energy of the cluster in its own potential is (Binney & Tremaine 1994, page 34)

$$E_c = 2\pi \int r^2 \rho(r) \Phi(r) dr. \quad (23)$$

We are only interested in the stars which become ejected after interacting with the binary, i.e. stars in the range between a_g and a_h . It is the energy of this fraction in the potentials of the cluster and the binary that we want to compare. Therefore we have to integrate Eq. (23) in the limits from a_g to a_h and obtain

$$E_c = -\frac{GM_c^2}{2r_c} \frac{1}{(1-1/\zeta)^2} \times \left[\frac{2}{\lambda} \frac{\eta-1}{\eta} - \frac{\ln \eta}{\zeta} + \frac{\ln \lambda}{\lambda} - \frac{\ln(\lambda\eta)}{\lambda\eta} \right]. \quad (24)$$

In this expression we used the following definitions

$$\eta \equiv \frac{a_h}{a_g}, \quad \zeta \equiv \frac{r_c}{r_i}, \quad \lambda \equiv \frac{r_c}{a_h}, \quad (25)$$

which can be combined to

$$\frac{a_h}{r_i} = \frac{\zeta}{\lambda}, \quad \frac{a_g}{r_i} = \frac{\zeta}{\lambda\eta}, \quad \frac{a_g}{r_c} = \frac{1}{\lambda\eta}. \quad (26)$$

The potential energy of this fraction of the cluster ($a_g \leq r \leq$

a_h) in the potential of the binary, which we approximated by that of a pointmass M_{12} at the origin, is

$$E_{\text{bin}} = -\frac{GM_{12}M_c}{r_c - r_i} \ln \frac{a_h}{a_g} = -\frac{GM_{12}M_c}{r_c} \frac{\ln \eta}{1 - 1/\zeta}. \quad (27)$$

This energy is obtained by multiplying the binding energy in Eq. (11) of Paper I with the factor 2. We assume that the mass of the cluster within the distance a_h corresponds to m_{ej} , i.e.

$$M(a_h) = M_c \frac{a_h - r_i}{r_c - r_i} = \frac{\mu}{k} \ln \frac{a_h}{a_g}. \quad (28)$$

Solving for the cluster mass and using the definitions in Eq. (25) we obtain

$$M_c = \frac{\mu}{k} \lambda \frac{\zeta - 1}{\zeta - \lambda} \ln \eta. \quad (29)$$

As we argued in Paper I solutions with $r_i < a_g$ are physically unreasonable because the mass in this range is not included in the mass which is interacting with and ejected by the binary. Therefore we assume $r_i = a_g$ in the following, implying $\zeta = \lambda\eta$. The ratio of the potential energies of the mass in the cusp range ($a_g \leq r \leq a_h$) then results in

$$\frac{E_c}{E_{\text{bin}}} = \frac{1}{k} \frac{q}{(1+q)^2} \left(1 + \frac{1}{2} \ln \lambda - \frac{\ln \eta}{\eta - 1} \right). \quad (30)$$

This ratio is plotted in Fig. 2 as a function of λ with the mass ratio q as parameter (bold lines) and $k = 1$. Since the dependency on η in Eq. (30) is very weak in the range $20 \lesssim \eta \lesssim 100$ we plotted the ratio only for $\eta = 50$. The figure clearly shows that the stars are bound much stronger in the potential of the binary than that of the cluster. The ratio increases with λ , but only for very large λ the energies become comparable, i.e. $\lambda \approx 500$ and $\lambda \approx 5 \times 10^9$ for $q = 1$ and 0.1, respectively. Such large clusters result in masses of about 2000μ and $2 \times 10^{10}\mu$ for $q = 1$ and 0.1, respectively, which are unrealistically large. Thus, even for major mergers it is justified to neglect the potential of the cluster with an index $\gamma = 2$ in order to compute the ejected mass that allows the BHs to merge.

In Paper I we showed that while the binary probably does not decay into the third phase if the density profile is as flat as $\gamma = 2$, it will enter the final phase for steeper profiles. Repeating the above analysis for a power law with the index $\gamma = 3$ we obtain for the cluster potential

$$\Phi_c(r) = -\frac{GM_c}{r} \begin{cases} \frac{r}{\ln(r_c/r_i)} \left(\frac{1}{r_i} - \frac{1}{r_c} \right), & 0 \leq r \leq r_i \\ \frac{1}{\ln(r_c/r_i)} \left(1 - \frac{r}{r_c} + \ln \frac{r}{r_i} \right), & r_i \leq r \leq r_c \\ 1, & r_c \leq r. \end{cases} \quad (31)$$

and hence for the energy of the cluster in its own potential in the range from a_g to a_h

$$E_c = \frac{GM_c^2}{r_c} \frac{1}{(\ln \eta)^2} (1 - \eta + \ln \eta). \quad (32)$$

In the same range the energy of the cluster in the potential of the binary is (Eq. (11) of Paper I multiplied with 2):

$$E_{\text{bin}} = -\frac{GM_{12}M_c}{\ln(r_c/r_i)} \left(\frac{1}{a_g} - \frac{1}{a_h} \right) = -\frac{GM_{12}M_c}{a_h} \frac{\eta - 1}{\ln \zeta}. \quad (33)$$

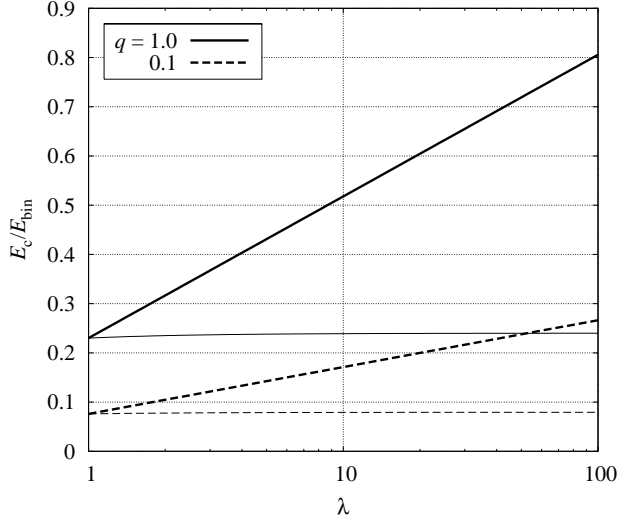


Figure 2. The energies of the cluster in the potential of the cluster itself and the binary as a function of the relative cluster size $\lambda = r_c/a_h$. The bold and thin lines are for flat ($\gamma = 2$) and steep ($\gamma = 3$) profiles, respectively. ($k = 1$, $\eta = 50$.)

Assuming as before that the mass m_{ej} is distributed in the cluster between a_g and a_h we obtain from Eqs. (4) and (9)

$$M_c = \frac{\mu}{k} \ln \zeta \frac{\ln \eta}{\ln(\zeta/\lambda)}. \quad (34)$$

For $r_i = a_g$ (i.e. $\zeta = \lambda\eta$) the ratio of the energies is

$$\frac{E_c}{E_{\text{bin}}} = \frac{1}{2k} \frac{q}{(1+q)^2} \left[2 - \frac{(\lambda+1) \ln \eta}{\lambda(\eta-1)} \right]. \quad (35)$$

This ratio is displayed in Fig. 2 by the thin lines. We can see that for the steeper profile the cluster potential contributes an even smaller fraction to the potential energy of the stars and increases much less with λ (i.e. is almost constant) than in the case of a shallower profile (bold lines). The steeper the density distribution, the stronger the stars are bound to the BHs. For a density distribution with a power law index as steep as $\gamma = 3$ the contribution of the self energy of the cluster is negligible, even in the limit of large ratios $\lambda = r_c/a_h$. The term in the square brackets of Eq. (35) then tends to $2 - \ln(\eta)/(\eta - 1)$, having a maximum of 2 if η tends to infinity so that the ratio E_c/E_{bin} approaches a maximum of $q/(1+q)^2$, what is 0.25 and only 0.083 for $q = 1$ and 0.1, respectively. While neglecting the cluster's potential is well justified for density profiles with $\gamma = 2$ it is an even better approximation for steeper mass distributions. Thus the results we obtained in Paper I should be a reasonably good approximation in the limit that the cluster contains a mass within the radius a_h which corresponds to about the binary's mass. Therefore we can be confident in our results which predict a successful merger of the BHs after the ejection of about m_{ej} .

5 MASS AND DENSITY PROFILE

The observed profiles of early type galaxies have been published in various papers. Lauer et al. (1995) casted the sur-

face brightness distributions into the ‘Nuker-law’, i.e. two power laws with inner and outer slopes which match at the break radius R_b . This is typically found on scales of some tens of parsecs or more. They detected a bimodal distribution and classified sources with slopes in the range $0 \leq \beta \lesssim 0.3$ as core galaxies while they referred to steep profiles with $\beta \gtrsim 0.5$ as power law galaxies. Deprojecting the surface brightness distributions Gebhardt et al. (1996) found the slopes of the luminosity density profiles to be in the range $0.3 \lesssim \gamma \lesssim 2.5$ peaking at 0.8 (core galaxies) and 1.9 (power law galaxies). Because the outer slope of both types is less than 3 it has to steepen again at large radii to keep the mass finite. This is not covered by the Nuker-law. Both classes of galaxies also differ in other respects (Lauer et al. 1995): Core galaxies have larger cores and are more massive and luminous with boxy or elliptical isophotes. They show a high velocity dispersion while they are slowly rotating. This is in agreement with this type of galaxies having undergone a major merger with redistribution of matter, dissipation of energy and cancellation of large amounts of angular momentum. This probably results in an increased central density at the time the binary becomes hard, as we argued in Paper I. Later Carollo et al. (1997); Rest et al. (2001); Ravindranath et al. (2001) found galaxies with intermediate slopes what might suggest that there is a smooth and continuous variation in the slopes and other properties of the galaxies.

More recently Graham et al. (2003) suggested a combination of a power law and Sérsic law to fit the surface brightness profiles. The new ‘Core-Sérsic’ model seems to generate better fits to the observed distribution, including the outer regions, and thus keeps the total mass finite. According to this model the galaxies previously classified as ‘power laws’ can be fitted by a pure Sérsic profile, while core galaxies follow a flat power law in the inner regions and a Sérsic profile at larger distances (Trujillo et al. 2004). The slopes of the inner power law are 20–40% larger compared to the Nuker-fits, while the break radii are smaller by a factor of ~ 2 –5. Thus the distribution of the slopes of the spatial profiles of the core galaxies peaks at about 1.14. Assuming a constant mass to light ratio we can use these models and their slopes for the density profiles.

5.1 Ejected mass & cluster mass

If the mass m_{ej} is distributed between a_g and a_h according to a power law with index $\gamma = 3$ its ejection allows the BHs to shrink to the final separation $a_f = a_g$ (Paper I). For flatter profiles we find $a_f > a_g$ while for steeper ones the BHs shrink into the range of phase 3, see Fig. 1 in that article. We also calculated how much mass m_{rq} exactly is required to be distributed between a_g and a_h for other slopes than $\gamma = 3$ in order to allow the binary to enter the final phase. This mass, expressed as a fraction of m_{ej} , is

$$\frac{m_{\text{rq}}}{m_{\text{ej}}} = \frac{2 - \gamma}{3 - \gamma} \frac{1 - \eta^{\gamma-3}}{1 - \eta^{\gamma-2}} \frac{\eta - 1}{\ln \eta} \quad (36)$$

such that for $\gamma = 3$ the ratio is equal to 1. If the amount of mass which is distributed in the cusp region, i.e. between a_g and a_h , is fixed the evolution of the merger in this phase and hence a_f does not depend on the extension of the cluster. However, changing the parameter $\lambda = r_c/a_h$ will influence

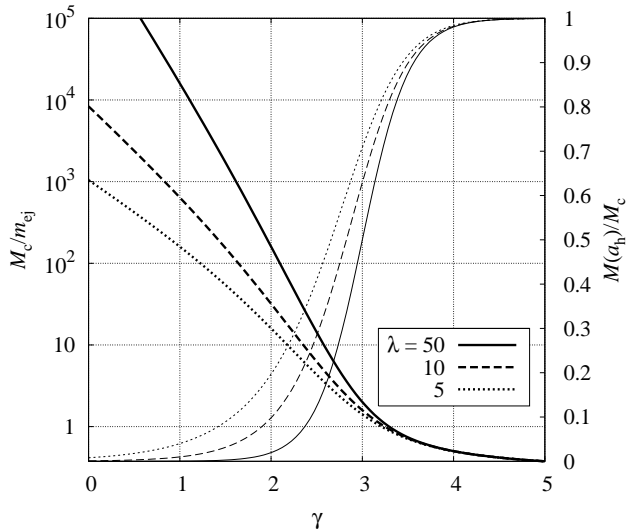


Figure 3. Bold lines, left-hand y -axis: The cluster mass in units of m_{ej} is shown under the condition that the mass within a_h is large enough to allow the binary to merge. Thin lines, right-hand y -axis: fraction of the cluster mass within a_h .

the total cluster mass. Scaled to the mass which is contained in the cusp, $M(a_h)$, we can express it as

$$\frac{M_c}{M(a_h)} = \frac{(\lambda\eta)^{3-\gamma} - 1}{\eta^{3-\gamma} - 1}, \quad (37)$$

assuming that the density distribution at larger radii has the same slope as in the cusp region. Deriving this mass ratio from Eq. (4) we again assumed that $r_i = a_g$ so that ζ can be replaced with $\lambda\eta$. If we require $M(a_h) = m_{\text{rq}}$ we can express the resulting cluster mass with the help of Eq. (36) in units of m_{ej} . This is plotted as function of the index γ in Fig. 3 (bold lines, left-hand y -axis). With m_{ej} being of the order of $10^8 M_\odot$ for a binary of a comparable mass (see Eq. (9)), Fig. 3 shows that for the BHs to merge the cluster has to be of about the same mass in case of steep profiles. The cluster mass is increasing with decreasing γ , the more steep, the larger the cluster is. It amounts to about $10^{10} M_\odot$ if $\gamma \approx 1.25, 1.6$ or 2.1 for $\lambda = 5, 10$ or 50 , respectively. Thus for large clusters with flat density profiles, as seen in core galaxies which are thought to have already undergone a major merger, the mass quickly becomes unphysically large, i.e. the binary would stall. But if the distribution is steep enough as we assume for an ongoing merger ($\gamma \gtrsim 2$) this problem does not occur.

Keeping the cluster mass fixed to m_{ej} and plotting the inverse of Eq. (37) we obtain the fraction of m_{ej} that is distributed within a_h and therefore accessible for ejection by the binary (thin curves in Fig. 3, scaled on the right-hand y -axis). We get the same curves if we restrict the cluster mass to m_{rq} instead of m_{ej} and then plot the cusp mass within a_h in units of m_{rq} . The mass fraction of the cusp is increasing with the slope. For a small γ the decay of the binary stops before the transition to the third phase is reached because there is not enough mass available for ejection (see also Fig. 1 of Paper I). The larger λ is, the less mass is contained within this range and the earlier the binary stalls.

For steeper distributions with $\gamma \gtrsim 2$ the fraction of ejected mass increases steeply with γ . Even for a cluster as large as $\lambda = 50$ this mass is sufficient for $\gamma \approx 3$ to allow the binary to shrink to a radius as small as about $2a_g$ (Eq. (12) of Paper I).

Comparing the ejected with the cluster mass we come to the same conclusion as before. For large clusters with shallow profiles its mass becomes unphysically large if the binary is supposed to enter the third phase. Therefore the decay of the binary would stall in core galaxies, which probably have already undergone a major merger. This is in good agreement with the conclusions drawn by Roos (1981) from his numerical three-body experiments. However, for steep profiles as we expect them to be formed during mergers, there is sufficient mass available for ejection without the cluster mass becoming too large, so that the BHs will coalesce. The post-merger profile has to match the observed mass distributions and comparing both we hope to obtain more information about the properties of the cusp.

5.2 Mass distribution during and after the merger

In Eq. (8) we can express the infinitesimal mass in terms of the density, $dm = 4\pi r^2 \rho(r) dr$, and rewrite this equation in the form

$$\frac{dm}{dr} = -\frac{\mu}{kr} = -4\pi r^2 \rho_{\text{ej}}(r). \quad (38)$$

Solving for the density distribution of the cusp we obtain

$$\rho_{\text{ej}}(r) = \frac{\mu}{4\pi k} r^{-3}, \quad (39)$$

i.e. a profile with a power law index $\gamma = 3$. This distribution represents the solution in Fig. 1 of Paper I, where for $\gamma = 3$ and $\lambda = 1$ all lines go through $a_f/a_g = 1$. This means that m_{ej} is distributed with just the right steepness that after its ejection the binary has shrunk to the semimajor axis a_g where gravitational radiation starts to dominate the further decay. With the slope $\gamma = 3$ the BHs eject the mass dm in the distance r owing to which the binary shrinks by an amount dr that corresponds precisely to the thickness of the spherical shell containing dm . If the density would fall below that of Eq. (39) somewhere in the range between a_g and a_h and we ignore the mass outside the shell $4\pi r^2 dr$, the binary would stall at this distance. For a steeper distribution more matter is bound deeper in the potential at smaller radii and its ejection would allow the binary to decay to radii smaller than a_g . If we assume that Eq. (39) is the initial profile, all the mass becomes ejected for $r \lesssim a_h$ and a hole remains in this range after the merger. But if the initial profile exceeds that of Eq. (39) we could subtract the latter from the former to compute the density distribution after the BHs have merged.

Non-core profiles

As Trujillo et al. (2004) showed, a Sérsic model is a very good approximation to surface brightness profiles, and assuming a constant mass to light ratio we can write for the surface density:

$$\Sigma(R) = \Sigma_0 \exp \left[-b \left(\frac{R}{R_e} \right)^{1/n} \right], \quad (40)$$

where R is the 2-dimensional radius and Σ_0 , R_e and n are parameters. While Σ_0 is just a scaling factor we can relate R_e to n if we require that a disc of radius R_e contains half of the total mass. Integrating Eq. (40) from the center to R_e and infinity the comparison of the obtained masses yields the relation $\Gamma(2n) = 2\Gamma(2n, b)$. Γ with one argument denotes the gamma function and with two arguments the incomplete gamma function, where we used the notation of Abramowitz & Stegun (1972). A good approximation to this relation is given by Prugniel & Simien (1997) with $b = 2n - 1/3 + 0.009876/n$. They also deprojected the surface density profile and gave a simplified fit to the spatial density distribution which can be written as

$$\rho_{\text{gal}}(r) = \rho_0 \left(\frac{r}{R_e} \right)^{-p} \exp \left[-b \left(\frac{r}{R_e} \right)^{1/n} \right]. \quad (41)$$

This is a Sérsic model multiplied with a power law where $\rho_0 = \Sigma_0/R_e$ and r is the 3-dimensional radius. The surface integral of Eq. (40) should give the same total mass as the volume integral of Eq. (41) and we obtain $\Gamma(2n) = 2b^{n(p-1)}\Gamma[n(3-p)]$. This allows to compute p as function of n . Márquez et al. (2000) give an updated version of the approximation by Lima Neto et al. (1999), $p = 1.0 - 0.6097/n + 0.05563/n^2$. Note that the half mass radius of the spatial distribution is slightly larger than of the surface profile, $r_e/R_e = 1.356 - 0.0293/n + 0.0023/n^2$ (Lima Neto et al.).

Non-core galaxies do not show signs of a recent merger like core galaxies. On the other hand the innermost data points used for fits are larger than a_h , and therefore a transition at this distance to a possible inner power law could not have been resolved. By the time the binary becomes hard we assume the mass to be distributed according to one of the following models: (a) According to the deprojected Sérsic model, which describes the resolved part very good and continues farther down to the center. After the BHs have merged we have to subtract the ejected cusp from the deprojected Sérsic profile, which therefore has to be at least as large as that of the ejected cusp at $r = a_g$. In model (b) the mass distribution is that of a deprojected Sérsic model with an additional cusp in the center when $a = a_h$, leaving behind a deprojected Sérsic profile after the BHs have ejected the cusp. The distribution of the ejected mass fraction in the cusp region for both models is:

$$\rho_\gamma = \rho_h \left(\frac{r}{a_h} \right)^{-\gamma} \quad (42)$$

It has to match Eq. (41) at $r = a_g$ and a_h for model (a) and (b), respectively. The volume integration of Eq. (42) over the cusp range yields the ejected mass fraction M_{ej} .

Equating both mass distributions at $r = a_g$ we obtain for the galaxy profile of model (a):

$$\rho_{\text{gal,(a)}} = \rho_h \frac{\eta^{\gamma-p}}{x^p} \exp \left\{ -b \left[\left(\frac{x}{x_e} \right)^{\frac{1}{n}} - \left(\frac{1}{\eta x_e} \right)^{\frac{1}{n}} \right] \right\}, \quad (43)$$

with $x = r/a_h$ and $x_e = R_e/a_h$. ρ_h is obtained from Eq. (3) using $r_0 = r_c = a_h$, $r_i = a_g$ and $M_c = M_{\text{ej}}$. We denote the term on the right hand side of the curly bracket of Eq. (3) with $g(\gamma, \eta)$ and thus find $\rho_h = g(\gamma, \eta) M_{\text{ej}}/(4\pi a_h^3)$. The volume integration then yields for the total mass of the galaxy

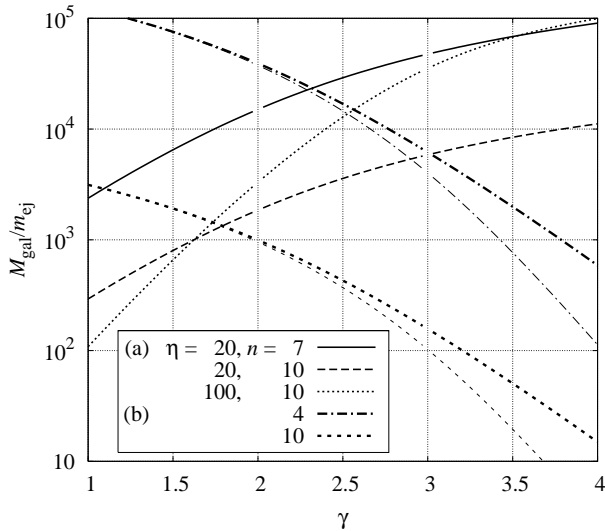


Figure 4. Mass of a non-core galaxy as function of the slope γ of the ejected profile. $x_e = 10^3$ and $m_{ej} \approx 10^8 M_\odot$. The bold and thin lines in model (b) are for $\eta = 20$ and 100 , respectively.

in units of the ejected mass

$$\frac{M_{gal,(a)}}{M_{ej}} = \eta^{\gamma-p} \frac{n x_e^{3-p}}{b^{n(3-p)}} g(\gamma, \eta) \Gamma[n(3-p)] e^{b(1/\eta x_e)^{1/n}} \quad (44)$$

For model (b) with the condition $\rho_\gamma(a_h) = \rho_{gal}(a_h)$ we obtain for the density and the mass:

$$\rho_{gal,(b)} = \rho_h \frac{1}{x^p} \exp \left\{ -b \left[\left(\frac{x}{x_e} \right)^{\frac{1}{n}} - \left(\frac{1}{x_e} \right)^{\frac{1}{n}} \right] \right\} \quad (45)$$

and

$$\frac{M_{gal,(b)}}{M_{cusp}} = \frac{n x_e^{3-p}}{b^{n(3-p)}} g(\gamma, \eta) \Gamma[n(3-p)] e^{b(1/x_e)^{1/n}}. \quad (46)$$

While the density given in Eq. (43) refers to the initial profile from which we have to subtract the cusp of Eq. (42) to obtain the final distribution, Eq. (45) is the expression for the final profile after the ejection of ρ_γ . Because the ejected mass is only a minor fraction of the total galaxy mass it does not make a difference whether we compare the initial or final galaxy masses. Note that they are actually lower limits for a successful merger. Assuming that $M_{ej} = m_{rq}$ of Eq. (36) we plot the galaxy mass in units of m_{ej} as function of the inner slope γ in Fig. 4. For all plots we used a ratio $R_e/a_h = 10^3$ because Trujillo et al. (2004) obtained for the fits of non-core galaxies half-light radii typically on the kpc scale. While we obtain ascending curves (solid, dashed, dotted) for model (a), they are descending (short dashed, dash-dotted) in case of model (b). If we keep the ejected mass of the cusp constant between a_g and a_h but increase the slope γ of its distribution the density increases at the inner edge, being compensated for by a decrease at the outer edge. Because the densities of model (a) and (b) match the cusp at a_g and a_h , respectively, we obtain the different dependencies on γ . For galaxies with a mass of some $10^{12} M_\odot$ or less Fig. 4 shows that possible solutions for model (a) with $\gamma \gtrsim 2$ require a large shape parameter $n \gtrsim 7$. We also find small cusps ($\eta \approx 20$) to be more likely than larger ones.

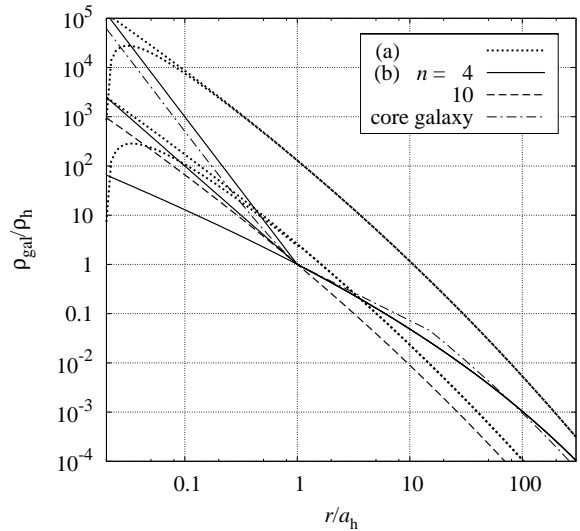


Figure 5. Density profiles. Model (a): The dotted lines with parameters $\gamma = 3$ and 2 (upper and lower pair, respectively). Initial and final profiles are the upper and lower branch of each pair. $n = 10, \eta = 50$. Model (b): solid lines from top to bottom: initial profiles with $\gamma = 3, 2$ and final profile for $n = 4$. Dashed line: final profile with $n = 4$. A core profile is shown by the thin dash-dotted line with $n = 6$.

If on the other hand an additional cusp is formed in the center when $a = a_h$ we do not find tight restrictions for the parameters. In the range $\gamma \gtrsim 2.5$ all shape parameters $n \gtrsim 4$ are possible. The size of the cusp η (20 and 100 for bold and thin lines, respectively) has only a small influence on the total mass of the galaxy. Trujillo et al. (2004) obtained for their best fits to non-core galaxies an average shape parameter of about 5. This basically excludes model (a) and is in very good agreement with steep cusps ($\gamma \gtrsim 2.5$) in model (b) so that shallower profiles seem to be less likely.

In Fig. 5, we plotted the density profiles for both models. The upper branch of both dotted pairs of curves shows the initial profile of model (a), i.e. a deprojected Sérsic model distribution with $n = 10$ and $\eta = 20$. After the BHs have coalesced and stars have been ejected from the center we obtain the lower branches as final profiles. For the upper and lower pair we used $\gamma = 3$ and 2 , respectively, for the ejected distribution. In the latter case we multiplied the final profile in the region $r < a_h$ with a factor of 1.5 in order to avoid a kink at $r = a_h$. This does not matter because Fig. 5 is meant to only give a rough idea about the possible shape of the profiles. Model (b): Both solid ($n = 4$) upper branches depict the initial profile for $\gamma = 3$ (top) and 2 . The lower branch is the final profile which is a pure deprojected Sérsic model and extends to the outer regions. The dashed line shows the final distribution for $n = 10$, which has a slope almost as steep as 2. The ratio of the initial and final mass contained in the cusp region varies between 1.8 and 3.3 for the parameters $(\eta, n) = (20, 10)$ and $(100, 4)$, respectively, if $\gamma = 2.5$. For $\gamma = 3$ we obtain a ratio between the limits 3.5 and 8.5 for the same sets of parameters. Hence this amount of mass has to be added to the mass of the relaxed profile in the cusp region during the merger if the BHs are to coalesce.

Our results suggest that if non-core galaxies are merger

remnants then model (b) is more likely than (a) and a cusp has been formed during the merger with an index $\gamma \gtrsim 2.5$ when $a = a_h$, which is subsequently removed by the merging BHs. This is also what we expect: It would be quite unlikely that an undisturbed deprojected Sérsic profile is maintained during the merger, especially when both cores merge and the binary becomes hard, without the formation of an inner cusp.

Core profiles

The surface brightness of core galaxies is well fitted by a Sérsic model in the outer parts and by a flat power law at distances smaller than the break radius R_b , see Trujillo et al. (2004). To keep things simple we will not try to deproject the core-Sérsic profile. Instead we use a power law with the index δ in the core region below the 3-dimensional break radius r_b , which we identify with R_b , and a deprojected Sérsic profile at larger radii, like Terzić & Graham (2005). For an infinitely sharp transition between both regimes the densities in the core and outer galaxy region can be written in the form:

$$\rho_{\text{core}} = \rho_b \left(\frac{x}{x_b} \right)^{-\delta} \quad (47)$$

$$\rho_{\text{gal}} = \rho_b \left(\frac{x}{x_b} \right)^{-p} \exp \left\{ -b \left[\left(\frac{x}{x_e} \right)^{\frac{1}{n}} - \left(\frac{x_b}{x_e} \right)^{\frac{1}{n}} \right] \right\}. \quad (48)$$

Here x denotes the radius in units of a_h so that $x_b = r_b/a_h$ and $x_e = R_e/a_h$. Both profiles match at x_b with the density ρ_b . Because Trujillo et al. found the slope of a core-Sérsic approximation to be about 30% steeper than Nuker fits in the core region we use $\delta = 1.14$ for the deprojected slopes instead of 0.8 what has been obtained by Gebhardt et al. (1996) when deprojecting Nuker fits. For the seven core galaxies of the sample of Trujillo et al. the average ratio of the half light radius and the break radius is $R_e/R_b \approx 70$. We assume that this ratio is roughly maintained for the deprojected spatial radii. Because R_e in this sample is typically on the kpc scale so that $x_e = 10^3$ we find for the spatial break radius $x_b \approx 15$, in units of a_h . For a flat core to be able to exist within r_b its slope has to be less steep than the slope α of the deprojected Sérsic profile evaluated at $x = x_b$:

$$-\alpha \equiv \frac{d \log \rho_{\text{gal}}}{d \log x} = - \left[p + \frac{b}{n} \left(\frac{x}{x_e} \right)^{1/n} \right] \quad (49)$$

The condition $\alpha > \delta$ is always fulfilled for $n \gtrsim 2$ and hence imposes no restrictions on our model. The break radius is larger by a factor of about 10 compared to a_h , which is on the parsec scale and thus very close to the radius of the innermost data point which has been used in the fits. Hence, if the profile of core galaxies is about the same at $r > a_h$ before and after the merger, it will have an additional cusp ρ_γ at $r < a_h$ when the binary becomes hard. By the time the BHs have coalesced we assume this cusp to have been removed and the profile of the core region ($a_h \leq r \leq r_b$) to extend also into the cusp region. Matching both profiles at $x = 1$ we obtain $\rho_b = \rho_h x_b^{-\delta}$ and find for the initial profile at $a_g \leq r \leq a_h$:

$$\rho_{\text{cusp}} = \rho_\gamma + \rho_{\text{core}} = \rho_h \left(x^{-\gamma} + x^{-\delta} \right). \quad (50)$$

The complete mass distribution of such a core galaxy from the cusp to the outer galaxy region is depicted by the thin

dash-dotted curve in Fig. 5 for the time when $a = a_h$. The used parameters are $\gamma = 3$, $\delta = 1.14$, $x_b = 15$, $x_e = 10^3$ and $n = 6$. Performing the volume integrations of all the components of the density profile over their respective regions we obtain for the masses:

$$M_{\text{cusp}} = M_{\text{ej}} \left[1 + g(\gamma, \eta) \frac{1 - \eta^{\delta-3}}{3 - \delta} \right], \quad (51)$$

$$M_{\text{core}} = M_{\text{ej}} g(\gamma, \eta) \frac{x_b^{3-\delta} - 1}{3 - \delta}, \quad (52)$$

$$M_{\text{gal}} = M_{\text{ej}} g(\gamma, \eta) \frac{x_e^{3-p}}{x_b^{\delta-p}} \frac{n}{b^{n(3-p)}} \Gamma \left[n(3-p), b \left(\frac{x_b}{x_e} \right)^{1/n} \right] \exp \left[b \left(\frac{x_b}{x_e} \right)^{1/n} \right]. \quad (53)$$

As before we used $\rho_h = g(\gamma, \eta) M_{\text{ej}} / (4\pi a_h^3)$ with $g(\gamma, \eta)$ being the term right of the curly bracket in Eq. (3) with $r_0 = r_c = a_h$ and $r_i = a_g$. For a successful merger we identify M_{ej} with m_{rq} of Eq. (36) and plotted the total mass of the galaxy $M_{\text{tot}} = M_{\text{cusp}} + M_{\text{core}} + M_{\text{gal}}$ in units of $m_{\text{ej}} \approx 10^8 M_\odot$ as function of γ in Fig. 6. We used $x_b = 15$, $x_e = 10^3$ and $\delta = 1.14$. The bold and thin lines are for $\eta = 100$ and 20, respectively, and from top to bottom we used as shape parameter $n = 4, 6$ and 10 for each set of curves. The figure shows that the lower mass limit that enables the BHs to merge decreases with increasing γ . Because the cusp profile has to match the flat core distribution at $r = a_h$, which in turn matches the deprojected Sérsic model at $r = r_b$, the mass of the core and galaxy region decreases with increasing γ . In fact, for flat cusps with $\gamma \lesssim 2$ the lower mass limit might actually be too large. While for $\gamma \lesssim 2.7$ small cusps with $\eta = 20$ result in smaller limits than $\eta = 100$ we find this reversed for steeper slopes. Trujillo et al. found shape parameters of $n \approx 5$ what argues for $\gamma \gtrsim 2.5$ and a transient cusp if the total mass should not exceed $10^4 m_{\text{ej}}$.

Instead of the deprojected Sérsic model we also used the Sérsic law of Eq. (40) for the spatial density distribution at $r > r_b$. We just replace R and R_e with r and r_e , respectively, and substitute Σ_0 with ρ_0 . If we use a three-dimensional Sérsic model at all radii the condition that a sphere of radius r_e contains half of the total mass leads to a very similar relation as in the 2-dimensional case between the factor b_3 in the exponent and the shape parameter n , $2\Gamma(3n, b_3) = \Gamma(3n)$. This can be approximated by $b_3 = 3n - 1/3 + 0.0079/n$ (Merritt et al. 2006). While the cusp and the core are the same as before we obtain for the mass in the region $r > r_b$ with the 3-dimensional Sérsic law

$$\frac{M_{\text{gal,s}}}{M_{\text{ej}}} = g(\gamma, \eta) \frac{x_e^3}{x_b^\delta} \frac{n}{b_3^n} \Gamma \left[3n, b_3 \left(\frac{x_b}{x_e} \right)^{1/n} \right] e^{b_3 (x_b/x_e)^{1/n}}. \quad (54)$$

This expression is also obtained by simply setting $p = 0$ and replacing b with b_3 in Eq. (53). The lower limit for the total mass of this model is shown by the dotted lines in Fig. 6 and is typically larger by a factor of a few compared to the deprojected Sérsic model. Hence the latter profile might be more appropriate for the mass distribution in galaxies which is derived from surface brightness profiles, while the former seems to describe galaxy sized dark matter halos slightly better (Merritt et al. 2006). On the other hand we can not identify the shape parameters of both models with each other

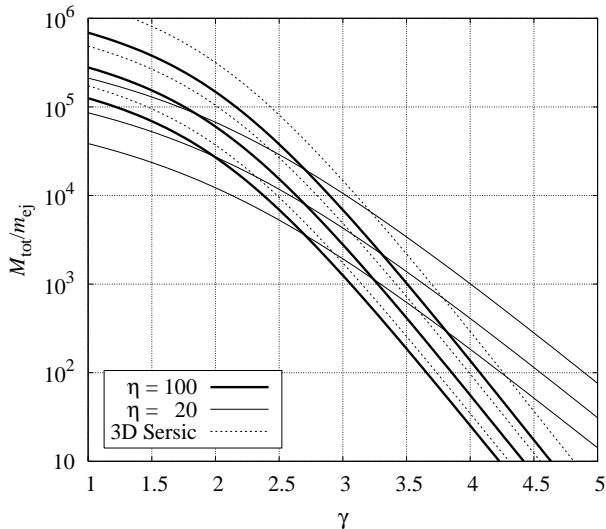


Figure 6. Total mass $M_{\text{tot}} = M_{\text{cusp}} + M_{\text{core}} + M_{\text{gal}}$ as function of the slope γ of the ejected profile. Fixed parameters are $(\delta, x_b, x_e) = (1.14, 15, 10^3)$. Each set of three curves is, from top to bottom, for the shape parameters $n = 4, 6$ and 10 . The solid lines are for the deprojected Sérsic profile and dotted lines for a three-dimensional Sérsic profile with $\eta = 100$. $m_{\text{ej}} \approx 10^8 M_{\odot}$.

and would expect n of the 3-dimensional Sérsic model to be slightly larger than n of the deprojected 2-dimensional Sérsic profile of the surface brightness. Thus the resulting curves should be closer to each other than shown in Fig. 6.

For both, non-core and core galaxies we find in Figs. 4 and 6 that for a successful merger generally less mass is required for large n . However, on average the sources considered by Trujillo et al. (2004) have a shape parameter of about 5 which is in favour of a steep cusp which is transiently formed (model (b) for non-core galaxies). If core galaxies are merger remnants such a cusp has been removed during the second phase. Constructing their profiles with an additional cusp at the time when the binary becomes hard yields galactic masses which are about $10^{12} M_{\odot}$ or less for $n \approx 5$, provided that the slope of the ejected mass distribution is $\gamma \gtrsim 2.5$. This confirms our conjecture that a steep cusp is formed transiently in the central regions and is in favour of core galaxies being rather the end product of a merger. However, in this simple model we would expect the break radius in the merger remnant to roughly coincide with a_h , the distance where the binary becomes hard. This is not clearly defined and a_h might actually be larger than assumed here. Maybe before the binary becomes hard the inner parts of the cluster surrounding each BH are so deeply bound in its potential that they increase the effective mass of the BHs. That would result in slingshot ejection of stars at larger radii before the naked BHs form a hard binary, i.e. a shift of a_h to larger distances. Increasing the size of the cusp at the expense of the core region, i.e. increasing a_h while keeping r_b constant, would shift the matching point of both profiles to larger radii where the steeper cusp profile has decreased to smaller values, see the core profile in Fig. 5. Consequently the mass of the matching core and galaxy region would decrease below the values shown in Fig. 6, so that M_{tot} becomes $\approx 10^4 m_{\text{ej}}$

even for $\gamma \approx 2$. It is also possible that the difference between a_h and r_b , of about a factor of 10, is caused by relaxation processes. We would expect a merger which shifts matter from the region inside a_h to larger distances also to change the steepness of the profile as well as to smooth out sharp transitions. In the post-merger profile the former transition between the ejected and remaining distribution might be much closer to the observed r_b than a_h . Eccentric orbits will also result in larger a_h , see the next Section.

In some galaxies the inner density profile has been observed to actually decrease towards smaller radii (Lauer et al. 2002). Depending on how close the ejected profile approaches the initial distribution all slopes less than the initial one, even holes in the profile, are possible in the merger remnant. The density distributions shown by Lauer et al. do not resemble a power law in the inner parts and are more similar to the profiles resulting from simulations of a fixed binary embedded in a stellar cluster (Fig. 1, Zier & Biermann 2001). Although these profiles would be in agreement with a stalled binary they could also be generated by completely merged BHs, depending on the initial distribution.

5.3 Possible deviations from the profile

According to our analysis the profile fulfills the following conditions when the binary becomes hard: It allows the BHs to merge completely without the cusp and galaxy becoming too massive and is generally in agreement with observed post-merger profiles after a fraction of the cusp has been ejected by the binary. In the cusp region the profile is steep ($\gamma \gtrsim 2.5$) turning into a power law at a_h with index $\delta \approx 1$ before it becomes a deprojected Sérsic profile at $r_b \approx 10 a_h$.

If the orbits of the stars in the cluster would be eccentric instead of circular, as we assumed, and we keep the pericenter fixed, the kick-parameter would be smaller (Eq. (7)). This would result in a larger mass which has to be ejected for coalescence (Eq. (9)), but also in a less steep cusp. Stars with apocenters $r_+ > a_h$ and pericenters $r_- \lesssim a_h$ will probably be close to r_+ , where they spend most of the time of the orbital period, when the binary becomes hard. Half a period later they interact with the BHs and can become ejected. These stars could compensate for the additional mass which is required for a successful merger for cusps with $\gamma < 3$. The ejection of these stars shifts a_h to larger radii and helps to explain the difference between a_h and the break radius because their apocenters populate the region between a_h and r_b . For apocenters $r_+ > r_b$ the eccentricity would become larger than $(r_b - a_h)/(r_b + a_h) \approx 0.8$, what might be unlikely. However, the exact shape of the initial profile will depend on the mass and velocity distributions in the isolated galaxies prior to their collision as well as on the orientation of both galactic spins and their orbital angular momentum relative to each other. The amount of dissipated energy, cancelled components of angular momentum and mass with low angular momentum which is funnelled into the central regions depend on these parameters. Each of the BHs will carry a stellar cusp of about its own mass. By the time the BHs become hard both cusps will have merged and together with other matter that has accumulated in the center they form a new massive and steep cusp. Fig. 3 of Milosavljević & Merritt (2001) suggests that the slope of this cusp is substantially

steeper than $\gamma = 2$. However, it needs to be clarified whether this is physical or due to spurious numerical relaxation. The post-merger profile will also be influenced by the time scale on which the binary decays in the second phase (Section 6). This will depend on the eccentricity of the BHB and also on the initial distribution of the mass and velocity of the stars in the cusp.

Our derivation above for the density distribution might be oversimplified because of the following possible deviations: A fraction of stars which has been ejected from the region $r \leq a_h$ will stay bound to the cluster, increasing the density at larger radii (Section 3.1). The binary also heats the remaining stellar population at $r \leq a_h$, further diminishing the cluster's density in this range. Due to the mass transfer from the inner to the outer regions of the cluster the stars which remain in the center are not as tightly bound as before and consequently extend to larger radii. All this redistribution of mass leads to a profile which is shallower than the difference between the initial and the ejected mass distributions. However, computing the difference between the core-Sérsic model and the Sérsic part extrapolated into the core region, Graham (2004) obtains mass deficits between 1 and 2 times M_{12} , depending on which method is used to determine the post-merger BH mass. Using Eqs. (9) and (36) we find for the ejected mass which allows the binary to enter the final phase:

$$\frac{m_{\text{req}}}{M_{12}} = \frac{q}{(1+q)^2} \frac{2-\gamma}{3-\gamma} \frac{1-\eta^{\gamma-3}}{1-\eta^{\gamma-2}} (\eta-1). \quad (55)$$

This ratio is displayed in Fig. 7 as function of q with the slope γ and the cusp size η as parameters. For a single major merger of a galaxy this is in very good agreement with the results of Graham. Deriving Eq. (55) we assumed efficient energy extraction via slingshot ejection (i.e. $\epsilon = 0$ and $k = 1$) and therefore consider the ratios in Fig. 7 as lower limits. Hence for mass ratios between 1 and 2 the cusp seems to be steeper than $\gamma = 2$ with $\gamma \gtrsim 2.5$ being more likely and thus strengthening our arguments.

5.4 Evolution time scale of an isolated cusp

A first approximation to the relaxation time of a collisionless system of particles is $t_{\text{relax}} \approx t_{\text{cross}} 0.1N / \ln N$ (Binney & Tremaine 1994), where t_{cross} is the crossing time and N the number of stars in the system. For our cluster with 10^8 stars, a size of about 1 pc and a typical velocity of $v_{\text{typ}} \approx \sqrt{GNm_*/a_h}$ we obtain a relaxation time of about 10^9 yr. However, the derivation of the expression of the relaxation time assumes a constant typical velocity for the cluster, which requires a density profile $\propto r^{-2}$. On the other hand the surface density is assumed to be constant as well, which is obtained for $\rho \propto r^{-1}$ for a distribution extending to $r = 0$. For a cusp with a profile as steep as $\gamma = 3$ the relaxation time will be shorter in the inner than in the outer regions and will also be affected by the boundary conditions.

A more precise expression for t_{relax} , which also takes into account encounters between stars, can be derived with the help of the diffusion coefficients in the Fokker-Planck approximation. We call this the diffusion time and following Binney & Tremaine (1994) we obtain

$$t_{\text{diff}} = \frac{\sqrt{6}}{4\pi} \frac{v^3(r)}{G^2 m_* \rho(r) \ln \Lambda}, \quad (56)$$

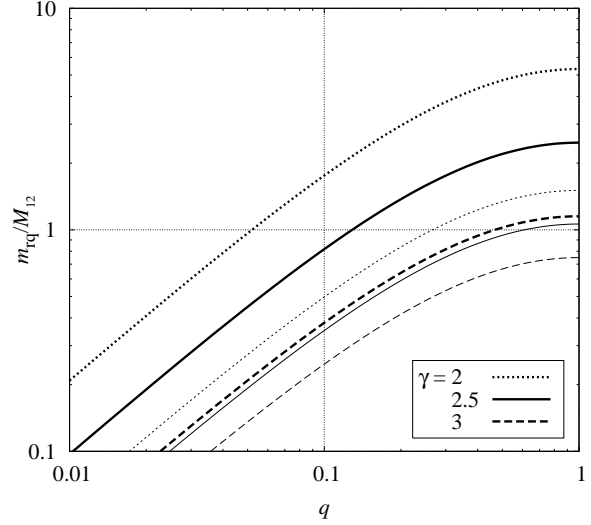


Figure 7. Ejected mass required for a successful merger is displayed in units of the mass of the binary as function of the mass ratio $q = m_2/m_1$. The bold lines are for $\eta = 100$, and the thin lines for $\eta = 20$.

with $\Lambda = b_{\text{max}} v_{\text{typ}}^2 / 2Gm_*$ and b_{max} being the maximum impact parameter, which is of the order of the size of the cusp. Because only the logarithm of Λ enters Eq. (56), even larger errors of Λ result only in minor errors of the diffusion time. However, the relaxation time depends sensitively on the velocity, which is of the order of the circular velocity $v_c = \sqrt{GM(r)/r}$. While for a steep cusp with $\gamma = 3$ the density in the denominator of Eq. (56) will diminish the diffusion time in the inner regions, the circular velocity counteracts this tendency and increases with decreasing r (being a factor of more than 3 larger for $\gamma = 3$ than for $\gamma = 2$ at $r \approx 3a_g$). Fig. 8 shows t_{diff} as a function of the radius for $\gamma = 2$ and 3. As expected the evolution times are much smaller at small radii for both slopes of the density distribution. Surprisingly the relaxation times of the steeper cusp (bold dashed curve) are larger than of the flatter cusp (bold dotted curve) over the whole plotted range, even at smaller radii. This is due to the strong dependency on the velocity. If we replot t_{diff} and keep the velocity fixed to $v_{\text{typ}} = \sqrt{GM_c/a_h}$ we obtain the thin curves, which are more consistent with our expectations: In the inner parts the steeper cusp evolves faster, but slower in the outer regions than a flatter distribution with $\gamma = 2$. The difference between both dotted curves, increasing towards the inner edge, is due to the influence of the cut-off at the inner boundary of the mass distribution on the circular velocity. However, a constant velocity all over the cusp region does not seem to be appropriate if the slope of the mass distribution is different from $\gamma = 2$.

To check this result we compare it with the time a star needs to spiral inwards from a distance $r > a_g$ to a_g due to dynamical friction. The decelerating force $F = m_* dv/dt$ is

$$F = -\frac{8\pi G^2 m_*^2 \rho(r) \ln \Lambda}{v_c^2(r)} \left(\text{erf}(\chi) - \frac{2\chi}{\sqrt{\pi}} e^{-\chi^2} \right), \quad (57)$$

with erf being the error function and $\chi \equiv v_c/(\sqrt{2}\sigma)$

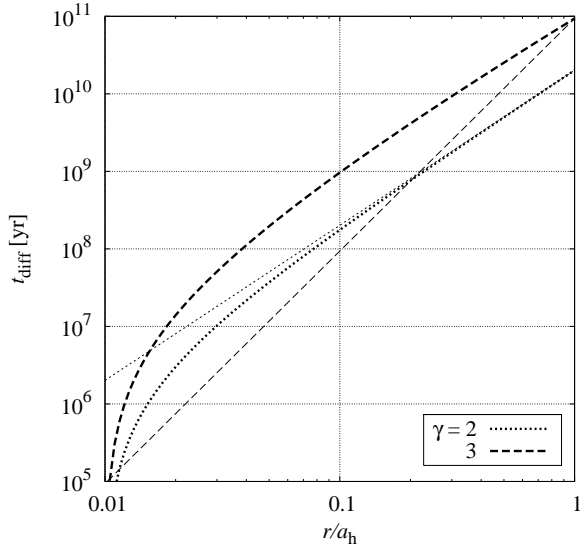


Figure 8. Relaxation time of the cusp as function of the radius, derived using diffusion coefficients. Bold lines: $v_c^2 \propto M(r)/r$, thin lines: $v_c = \text{const}$.

(Binney & Tremaine). This force is tangential to the orbit and therefore causes the star to lose angular momentum per unit mass at a rate

$$\frac{dl_*}{dt} = \frac{Fr}{m_*}. \quad (58)$$

The star continues to orbit at the speed $v_c(r)$ as it spirals into the center with an orbital angular momentum per unit mass $l_* = rv_c$. If $\gamma = 2$ and the cusp extends to the origin the circular velocity is constant. The integration of Eq. (58) yields for the time to spiral inwards from an initial radius r_{in} to a_g

$$t_{\text{fric}} = \frac{v_c^3}{8\pi G^2 m_* S(\chi) \ln \Lambda} \frac{x_{\text{in}}^\gamma - \eta^{-\gamma}}{\gamma \rho_0}. \quad (59)$$

Here $S(\chi)$ is just an abbreviation for the term in the brackets of Eq. (57), and x is the radius in units of a_h . If the distribution has an inner boundary at a_g the circular velocity is not constant anymore what has to be taken into account in the time derivative of l_* in Eq. (58). Then the time to spiral to the inner boundary becomes

$$t_{\text{fric}} = \frac{Q}{2\eta^2 \sqrt{1-1/\eta}} \left[\eta(2\eta x_{\text{in}} - 3) \sqrt{x_{\text{in}}(x_{\text{in}} - 1/\eta)} + \ln(\sqrt{\eta x_{\text{in}}} + \sqrt{\eta x_{\text{in}} - 1}) \right], \quad (60)$$

with $Q = \sqrt{Na_h^3/(Gm_*)}/(4S(\chi) \ln \Lambda) \approx 4 \times 10^9 \text{ yr}$ for our cusp and $M_c = Nm_*$. Also for $\gamma = 3$ the circular velocity depends on r . Integrating and solving for the time yields

$$t_{\text{fric}} = \frac{2a_h}{12\pi S(\chi) \ln \Lambda} \sqrt{\frac{N}{Gm_*}} \frac{\ln(x_{\text{in}}\eta)}{\ln \eta} x_{\text{in}}. \quad (61)$$

Plotting t_{fric} in the same way as t_{diff} in Fig. 8 we obtain very similar curves whith only slightly smaller times. Thus the relaxation time due to dynamical friction is in very good agreement with the time obtained using diffusion coefficients, confirming a larger relaxation time for steeper profiles. For both

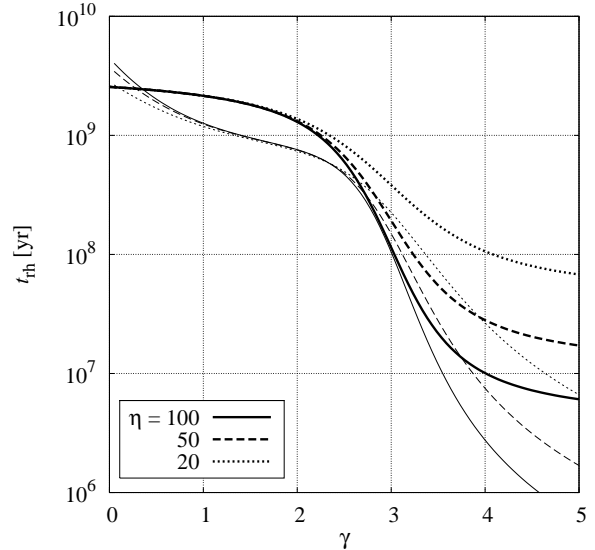


Figure 9. The median relaxation time as a function of the cusp's slope. The bold curves have been derived using the diffusion coefficients while for the thin curves the dynamical friction formalism has been used, see Eq. (62).

results the relaxation time quickly drops to zero as the inner boundary of the distribution is approached. This is just a consequence of our assumption that the mass distribution does not extend to smaller radii than a_g . However, real cusps will not have such a sharp cut-off and their profiles will extend into the inner regions, although with a slope less steep than $\gamma = 3$ (the mass has to be finite), resulting in times larger than those shown in Fig. 8.

To avoid these problems we try to characterize the cusp by a single relaxation time, as suggested by Binney & Tremaine (1994), and replace the density by the mean density $\rho_h = \frac{1}{2}M_c/(\frac{4}{3}\pi r_h^3)$ inside the cusp's half-mass radius r_h . The mean-square speed of the stars is best described by $\langle v^2 \rangle \approx 0.4GM_c/r_h$, and we use $\Lambda = r_h \langle v^2 \rangle / Gm_* = 0.4N$. For the diffusion and friction time we then obtain

$$t_{\text{diff},h} = \frac{\sqrt{6}}{4\pi} \frac{\langle v^2 \rangle^{3/2}}{G^2 m_* \rho_h \ln \Lambda} \quad (62)$$

$$t_{\text{fric},h} = \frac{\langle v^2 \rangle^{3/2}}{8\pi G^2 m_* S(\chi) \ln \Lambda} \frac{x_h^\gamma - \eta^{-\gamma}}{\gamma \rho_0},$$

where the half-mass radius in dependency of the slope is

$$x_h = \frac{r_h}{a_h} = \begin{cases} \left(\frac{1+\eta^{\gamma-3}}{2} \right)^{1/(3-\gamma)}, & \gamma \neq 3 \\ \frac{1}{\sqrt{\eta}}, & \gamma = 3, \end{cases} \quad (63)$$

and ρ_0 is taken from Eq. (3). Note that for $\gamma = 3$ the half-mass radius is the geometrical mean of a_g and a_h , i.e. $r_h = \sqrt{a_g a_h}$. The dependency of these times on the slopes with η as parameter is shown in Fig. 9. On average the diffusion coefficients (bold lines) yield slightly larger relaxation times than dynamical friction (thin lines). Both times decrease with increasing slopes, as might be expected, and increase with decreasing η , i.e. increasing a_g . While for small γ the relaxation time does not sensitively depend on the slope it

quickly decreases at $\gamma \approx 3$ before becoming flatter again at $\gamma \gtrsim 4$. For both methods we find t_{relax} to be in the range between 10^8 and 10^9 yr for a slope in the range $2 \lesssim \gamma \lesssim 3$. In the following we assume that a cusp with $\gamma \approx 3$ is conserved for less than 10^9 yr.

The strict conservation of the slope $\gamma = 3$ is only necessary in the theoretical derivation of Eq. (39). We assumed the stars to move on circular orbits and that the binary can only eject those stars whose radius corresponds to the current semimajor axis. For elliptical stellar orbits the distribution could be flatter and extend to larger radii, but a more massive cusp would be required for coalescence due to a smaller binding energy, as explained previously. Once the binary has become hard it will influence all stars moving at smaller radii than a . If the inner parts of the cluster collapse, maybe even into a third BH, its mass will become bound more deeply in the potential of the binary and hence its ejection will extract more energy. Only if these stars are so deeply bound in the potential of one of the BHs that the perturbations caused by the secondary are negligible the merger might stop. Therefore the BHs might still coalesce when the time since they have become hard exceeds a couple of 10^8 yr and a $\rho \propto r^{-3}$ profile is not conserved. We may conclude that the binary covers the second phase when it decays from a_h to a_g in the time $t_{\text{hg}} < 10^9$ yr.

6 TIME DEPENDENCY OF THE MERGER

With our approach to compute the required stellar mass for a successfully merging BHB we can not determine the rate at which stars are ejected and consequently no shrinking rate of the binary. To derive the time dependency of the merger we would have to make further assumptions about the rate at which stars interact with and are ejected by the BHs, i.e. about the velocity distribution of the stars. This might be quite difficult during an ongoing merger. Nevertheless, one assumption we want to make is that the shrinking rate is constant once the binary has become hard,

$$H \equiv \frac{d}{dt} \left(\frac{1}{a} \right) = \text{const.} \quad (64)$$

This behaviour has been observed for hard binaries and a full loss-cone in various numerical experiments (Hills 1983; Quinlan 1996; Milosavljević & Merritt 2001; Zier & Biermann 2001) and should therefore also be applicable for steep and compact cusps and to triaxial galaxies whose loss cone is always full (Yu 2002; Holley-Bockelmann et al. 2002; Holley-Bockelmann & Sigurdsson 2006; Berczik et al. 2006). Note that our definition is different from that used by Quinlan (1996) who defined the shrinking or hardening rate as a dimensionless quantity. We assume that the binary needs the time t_{hg} to shrink from the initial semimajor axis a_h to a_g . Integrating Eq. (64) in time from $t = 0$ to some time $t < t_{\text{hg}}$ and in distance from a_h at $t = 0$ to $a(t)$, respectively, we can solve for the semimajor axis which the binary has reached after the time t has elapsed and obtain

$$\frac{a(t)}{a_h} = \frac{1}{1 + H a_h t}. \quad (65)$$

If $t = t_{\text{hg}}$ the binary has shrunk to a_g and solving for the hardening rate yields $H = (\eta - 1)/a_h t_{\text{hg}}$. Applying this to

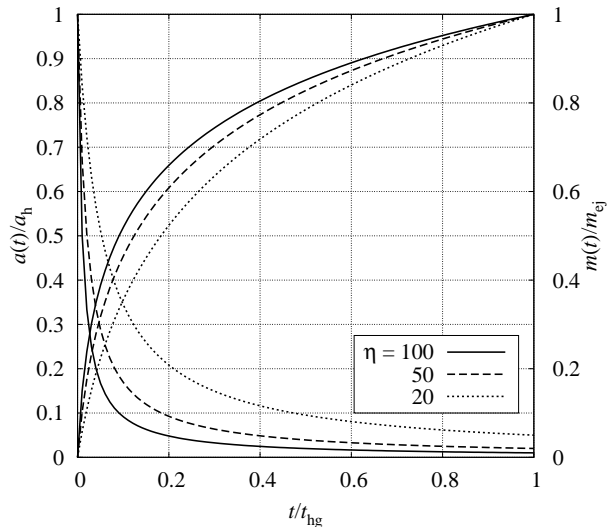


Figure 10. Evolution of the semimajor axis (decreasing curves) and the ejected mass (increasing curves) with time. The shrinking rate is assumed to be constant.

Eq. (65) we can rewrite the semimajor axis in the form

$$\frac{a(t)}{a_h} = \frac{1}{1 + (\eta - 1)t/t_{\text{hg}}}. \quad (66)$$

The integration of Eq. (8) gives the mass which has been ejected by the time the semimajor axis has shrunk to $a(t)$ and we only need to replace a_g with $a(t)$ in Eq. (9) to obtain an expression for $m(t)$. With the help of Eq. (66) we can write the time dependency of the ejected mass as

$$\frac{m(t)}{m_{\text{ej}}} = \frac{\ln [1 + (\eta - 1)t/t_{\text{hg}}]}{\ln \eta}. \quad (67)$$

Both functions are plotted in Fig. 10 for different ratios η . The increasing curves show the mass evolution and the decreasing ones show the change in the semimajor axis with time. In the beginning the evolution of the binary is fastest, especially the decay of the semimajor axis. It has decreased to $1/5$ or less of its initial value after only $\sim 1/5$ of the merging time t_{hg} . In the same period the ejected mass amounts to more than a half of the total mass m_{ej} which the BHs have ejected once they reach the separation a_g . After a time of about $0.2 t_{\text{hg}}$ has elapsed the evolution slows down noticeably and the binary spends most of its time in the second phase to shrink the remaining distance from less than $0.2 a_h$ to $a_g = a_h/\eta$. Hence, if a binary really stalls it will be most likely found in the range $a_g \lesssim a \lesssim 0.2 a_h$, see Section 8. This is in agreement with the results of the numerical three-body experiments by Roos (1981) which suggest that the binary stops shrinking at a separation of the BHs of about $0.015 r_{\text{cusp}}$.

Initially the mass ejection rate is $\dot{m}(0) = \mu(\eta - 1)/(k t_{\text{hg}})$ and exceeds the rate at the end of the second phase when $t = t_{\text{hg}}$ by a factor of η . This is probably the time when the BHB carves a torus comprised of stars out of the initial stellar distribution (Zier & Biermann 2001, 2002). In Section 5.4 we showed that the steep profile of the cusp is conserved for some 10^8 yr, and therefore the binary should shrink from a_h to a_g on a similar time scale or less. Taking $t_{\text{hg}} = 5 \times 10^8$ yr

and assuming a mass ratio $q = 1$ with $m_1 \approx 10^8 M_\odot$ we obtain an initial ejection rate of about 2, 5 and $10 M_\odot/\text{yr}$ for $\eta = 20, 50$ and 100 , respectively. At the end of phase 2 the ejection rate is smaller by a factor of $1/\eta$ and amounts only to $0.1 M_\odot/\text{yr}$, being almost independent of η for $\eta \gg 1$. This again indicates that the evolution at the end of phase 2 is much slower than in the beginning.

We have not taken into account any dependency on the density profile and velocity distribution. While the shrinking rate might still be a constant due to a filled loss-cone, the shrinking time t_{hg} probably depends on both distributions. This could be explored in more detail with the help of N -body simulations. From our estimates in Section 5.4 of the relaxation time of the cusp we deduced a time t_{hg} less than 10^9 yr. Another estimate for the order of magnitude of t_{hg} could also be derived from Z-shaped radio galaxies, as has been pointed out by Zier (2005), but that is beyond the scope of the present paper.

7 m_{ej} IN MULTIPLE MERGERS

Although our approach to the merger of a massive BHB is quite simple the results seem to describe such a merger reasonably well. However, there is a simple and easy consistency check with numerical simulations which we want to carry out. According to simulations more mass is ejected if the primary BH merges N times with a BH of mass m_1/N than in one merger with a secondary BH of mass $m_2 = m_1$ (e.g. Quinlan 1996; Zier & Biermann 2001). In case of one merger we have $m_{\text{ej}} = m_1 \ln(a_{\text{h}}/a_{\text{g}})/(2k)$, cf. Eq. (9) with $q = 1$. If we distribute the merging mass over N mergers we have $m_2 = m_1/N$. When the i th merger proceeds, the primary's mass is that it has after the $(i-1)$ th merger has been completed,

$$m_{1,i} = m_1 + \frac{i-1}{N}m_1 = m_1 \frac{N+i-1}{N}. \quad (68)$$

The mass ratio during the i th merger then is

$$q_i = \frac{m_2}{m_{1,i}} = \frac{1}{N+i-1}, \quad (69)$$

and hence the reduced mass $\mu_i = m_{1,i} q_i / (1 + q_i)$. Thus we can write the mass which becomes ejected during the i th merger as

$$m_{\text{ej},i} = \frac{m_1}{k} \ln \left(\frac{a_{\text{h}}}{a_{\text{g}}} \right) \frac{1}{N} \frac{N+i-1}{N+i}. \quad (70)$$

The total mass ejected in N mergers then amounts to

$$m_{\text{ej,tot}} = \sum_{i=1}^N m_{\text{ej},i} = \frac{m_1}{k} \ln \left(\frac{a_{\text{h}}}{a_{\text{g}}} \right) \frac{1}{N} \sum_{i=1}^N \frac{N+i-1}{N+i}. \quad (71)$$

The sum on the right hand side is equal to $N + \psi(1+N) - \psi(1+2N)$, where ψ is the Psi (Digamma) Function and can be approximated by $N^2/(1+N)$, with a maximum error of about 6% for $N = 2$. This approximation corresponds to keeping i fixed to 1 in the above expression for $m_{1,i}$ so that $m_{1,i}$ remains constant at $m_{1,i} = m_1$ for all mergers. Hence the primary's mass is fixed and its growth with the increasing number of mergers can be neglected. The total ejected mass after N mergers is approximately

$$m_{\text{ej,tot}} \approx \frac{m_1}{k} \frac{N}{1+N} \ln \frac{a_{\text{h}}}{a_{\text{g}}} \quad (72)$$

and the ratio of the mass ejected in N mergers with $m_2 = m_1/N$ compared to one merger with $m_2 = m_1$ is

$$\frac{m_{\text{ej,tot}}}{m_{\text{ej}}} = 2 \frac{N}{1+N}. \quad (73)$$

This is a function that grows with N , in agreement with the results of numerical simulations. In deriving this ratio we neglected the dependency of $\eta = a_{\text{h}}/a_{\text{g}}$ on the mass ratio q . According to numerical experiments this ratio is increasing with decreasing q . Therefore, the inclusion of this dependency would result in an ejected mass which increases more steeply with N , making our result more pronounced.

8 ONGOING MERGERS

The results we obtained in the present article and Paper I suggest that the BHB which forms after the collision of two galaxies most likely merges. In the introduction we cited observational evidence for ongoing mergers where the BHs are still orbiting around each other. It has been pointed out by Gopal-Krishna, et al. (2003) that in ZRGs during the time between the bending of the pre-merger jet into a Z-shape by the secondary galaxy and the launching of the post-merger jet after the coalescence of both BHs we should see only the pure Z-shape, but no complete X-shape of the jets. So far no galaxies with a pure Z-shape have been observed. In the new and strongly increased sample of XRGs, compiled by Cheung (2007), about three such sources out of hundred galaxies might have been observed for the first time, i.e. J0145-0159, J1040+5056 and J1206+3812. Of course this needs a thorough and detailed analysis. However, even the existence of these objects would not indicate that the binary has stalled and is rather a sign that the separation of the BHs is somewhere below 30-100 kpc (Zier 2005), therefore providing a very important laboratory for the research of ongoing mergers and merger history. The sample of Cheung also seems to increase the number of post-merger ZRGs, supplying more objects for the deprojection of the jets as has been done by Zier (2005). The pure Z-shaped sources might be good candidates to look for a spatially resolved binary like in NGC 6240 which has been discovered by Komossa et al. (2003). Because of the projected separation of the BHs of about 1.4 kpc this merger is currently in the first phase. More recently Rodriguez et al. (2006) have discovered a black hole binary with a total mass of $\sim 1.5 \cdot 10^8 M_\odot$ and a projected separation of only 7.3 pc in the radio galaxy 0402+379, probably the most tightly bound binary that has been observed directly so far. The elliptical host galaxy shows signs of a recent merger and the two nuclei appear to be active, suggesting ongoing accretion and dissipation. Because the separation is seen in projection it is rather a lower limit and therefore the merger is still in the first phase or at most at the beginning of the second when the loss-cone is still full. Hence, this is another example of an ongoing merger where the loss-cone is not depleted. However, based on numerical simulations of a BHB in a stellar core some authors claimed that probably the binary stalls in the second phase due to loss-cone depletion (e.g. Quinlan 1996; Makino 1997; Quinlan & Hernquist 1997; Milosavljević & Merritt 2001; Berczik et al. 2005). To test this prediction, which contradicts ours of successfully coalescing BHs, we look for ongoing mergers which happen

Table 1. Sources exhibiting (semi)periodic changes in lightcurves, possibly due to a BHB. Columns: (1) source, (2) redshift, (3) intrinsic period, (4)-(7) BH masses, (8) current separation scaled to a_g in units of 10^{-3} ($q = 0.1$), (9) mass ratio obtained under the condition that $a = a_g$, and (10) remaining time to coalesce due to emission of gravitational waves ($q = 0.1$).

Source	z	T_{intr} [yr]	$\log(M_{\text{BH}}/M_{\odot})$		a/a_g [10^{-3}]	$a = a_g$ $-\log(q)$	$a = a_g$ $\log(t_g/\text{yr})$		
(1)	(2)	(3)	(4)	(5)	(6)	(7)	(8)	(9)	(10)
Mrk 421	0.031	22.4			7.6	8.3^{σ}	373 - 730	2.7 - 1.6	8.3 - 9.5
Pks 0735+178	0.424	10.0	8.1	8.3	8.2		218 - 264	3.7 - 3.3	7.4 - 7.7
BL Lac	0.069	13.1	6.4	7.3	7.7	8.4^{σ}	237 - 1615	3.5 - 0.01	7.5 - 10.8
On 231	0.102	12.3			8.0		334	2.9	8.1
Oj 287	0.306	9.1	7.7	8.4	8.1	8.8^{λ}	127 - 364	4.6 - 2.8	6.4 - 8.3
Pks 1510-089	0.361	0.7			8.0	8.6^{λ}	27.8 - 49.4	7.2 - 6.2	3.8 - 4.8
3C 345	0.595	6.3			8.0	9.3^{λ}	61.4 - 214	5.9 - 3.7	5.2 - 7.3
AO 0235+16	0.940	2.9	8.7	8.7	8.0		65.1 - 127	5.8 - 4.6	5.3 - 6.4
3C 66A	0.444	0.125			8.0		15.7	8.2	2.8
Mrk 501	0.033	0.063			8.3	9.2^{σ}	3.14 - 7.43	11 - 9.5	-0.01 to 1.5
3C 273	0.158	0.00225			9.0	9.2^L	0.34 - 0.41	15	-3.9 to - 3.5
Sgr A*	0.0	0.3		$6.5^{(e)}$	$6.6^{(f)}$		108 - 118	4.9 - 4.7	6.1 - 6.3

References for the periods: Mrk 421 (Liu et al. 1997), Pks 0735+178 (Fan et al. 1997), BL Lac (Fan et al. 1998), On 231 (Liu et al. 1995), Oj 287 (Pursimo et al. 2000), Pks 1510-089 (Xie et al. 2002), 3C 345 (Zhang et al. 1998), AO 0235+16 (Raiteri et al. 2001), 3C 66A (Lainela et al. 1999), Mrk 501 (Hayashida et al. 1998), 3C 273 (Xie et al. 1999), Sgr A* (Zhao et al. 2001). *References for the masses:* With the exception of Sgr A* the values in columns (4) and (5) were taken from Xie et al. (2002), in column (6) from Xie et al. (2004) and in column (7) from Wang et al. (2004). Masses for Sgr A* are from ^(e) Schödel et al. (2003) and ^(f) Ghez et al. (2003). The indices σ , λ , L indicate the method used to determine the BH mass. See text for details.

to be in the second phase. These might still not be stalled and actually en route to coalescence. Only if there is a significant number of ongoing mergers in the second phase, preferentially in the range $a_g \lesssim a \lesssim 0.2 a_h$ as we predicted in Section 6, this could indeed argue for a stalled binary. A still existing BHB manifests itself also in semi-periodic signals in lightcurves, see Komossa (2003, 2006) and references therein. Katz (1997) presented a model for OJ 287 where the precession of the accretion disc, driven by the gravitational torque of the secondary BH, causes the jet to sweep periodically across our line of sight. Doppler-boosting leads to the observed variations of the luminosity and the period of the binary is much less than the 9 yr interval of the luminosity variations in the rest frame of the galaxy. Models by Sillanpää et al. (1988) and Valtaoja et al. (2000) relate the variations of the lightcurve to interactions of the secondary BH with the accretion disc and therefore the observed period corresponds to the orbital period of the binary. Merritt & Milosavljević (2005) have compiled a sample of active galaxies whose observed periodic variabilities might be related to the orbital motion of the BHs. We assume that the intervals of these variabilities correspond to the period of the binary and use them together with independent estimates for the mass of the BHs to determine the separation of the BHs and hence the phase in which the merger has been observed. Kepler's third law relates the binary's period T to its semimajor axis,

$$T = 2\pi \sqrt{\frac{a^3}{GM_{12}}}. \quad (74)$$

We scale a with the semimajor axis where gravitational waves start to dominate the decay of the binary, a_g . For circular orbits this is (Peters 1964)

$$a_g = \left[\frac{256}{5} \frac{G^3 \mu M_{12}^2}{c^5} t_g \right]^{1/4}. \quad (75)$$

Note that Peters (1964) actually gave this expression in the form $\langle da/dt \rangle = -(64/5) G^3 \mu M_{12}^2 / (c^5 a^3)$ which integrated yields Eq. (75). Some authors alternatively used the definition $t_g \equiv |\dot{a}/a|^{-1}$ evaluated at $a = a_g$ which differs from t_g in Eq. (75) by a factor of 4. Combining Eqs. (74) and (75) we obtain for the current semimajor axis in units of a_g :

$$\frac{a}{a_g} = \frac{1}{29} \left(\frac{m_1}{10^8 M_{\odot}} \right)^{-\frac{5}{12}} \left(\frac{t_g}{10^{10} \text{ yr}} \right)^{-\frac{1}{4}} \left(\frac{T}{\text{yr}} \right)^{\frac{2}{3}} \frac{(1+q)^{\frac{1}{2}}}{q^{1/4}}. \quad (76)$$

Because of the small exponent 1/4 the semimajor axis depends only weakly on the time. Scaling t_g with 10^8 yr instead of 10^{10} yr increases a by only a factor of ~ 3 . The period T and the mass m_1 of the primary BH of the binary we derive from observations. Assuming a mass ratio q then allows us to compute the separation of the BHs. In Table 1, we listed the sources in column (1) and used their redshifts (2) to transform the observed periods into the rest frame of the source via $T_{\text{intr}} = T_{\text{obs}}/(1+z)$, column (3). For the central BH mass we found different values in the literature which have been obtained with various methods (columns (4) to (7)). Xie et al. (2002) assume a maximally rotating Kerr BH and relating the observed minimal timescales of the luminosity variations, on scales between 1/2 to 12 hours, to the period of the marginally bound orbit they obtain an upper limit of the BH mass which is given in column (5). The same authors used an expression for the Eddington-limit that includes the Klein-Nishina effects on the Compton scattering cross Section to obtain a lower limit for the mass, listed in column (4), a method proposed by Dermer & Gehrels (1995). Later Xie et al. (2004) used again the method of the minimal timescales for a larger sample with the results shown in column (6). Wang et al. (2004) employed three different methods to determine the central BH mass which is indicated by the upper index in column (7). They either used

the $M_{\text{BH}} - \sigma$ relation as fitted by Tremaine et al. (2002) (σ), the linewidth-luminosity-mass scaling relation (Kaspi et al. 2000) (λ), or the correlation between the luminosity of the host galaxy and BH mass (McLure & Dunlop 2001) (L). For Sgr A* Ghez et al. (2003) and Schödel et al. (2003) used observations of absorption lines to determine the orbits of central stars and hence the mass of the BH.

As can be seen in Table 1 the masses for some objects are quite different by up to a factor of 100 (BL Lac, 3C 345, Oj 287). There is also a contradiction for AO 0235+16 between the lower and upper limits of the mass in columns (4) and (6), respectively, and between columns (6) and (7), where the latter mass is not supposed to be an upper limit. Notwithstanding these problems we just took the smallest and largest mass and computed the corresponding range of the current separation of the BHs using Eq. (76) with $q = 0.1$. The result is given in column (8) in units of 10^{-3} . For $q = 1$ the obtained semimajor axes would be even smaller by a factor of 0.6. Assuming that the binary's current semimajor axis is just at the transition from phase 2 to 3, i.e. $a = a_g$ we can solve Eq. (76) for the required mass ratio q and obtain

$$q = \frac{3^{1/3} 2\chi + 2^{1/3} (\sqrt{3\chi^2(27-4\chi)} + 9\chi)^{2/3}}{6^{2/3} (\sqrt{3\chi^2(27-4\chi)} + 9\chi)^{1/3}}. \quad (77)$$

Here we used the definition

$$\chi^{1/12} \equiv (4\pi^2)^{-1/3} c^{5/4} (Gm_1)^{-5/12} T^{2/3} t_g^{-1/4}. \quad (78)$$

The negative logarithm of the mass ratio is tabulated in column (9). Binaries with a smaller mass ratio are still in phase 2, while for larger ratios gravitational radiation already dominates the decay. In the last column we listed the remaining time for the BHs to merge due to emission of gravitational waves if $q = 0.1$, which is obtained by solving Eq. (76) for t_g with $a = a_g$,

$$t_g = 1.5 \cdot 10^4 \left(\frac{m_1}{10^8 M_\odot} \right)^{-5/3} \left(\frac{T}{\text{yr}} \right)^{8/3} \frac{(1+q)^{1/3}}{q} \text{yr}. \quad (79)$$

For $q = 1$ this time is shorter by a factor of about 0.12.

The results show very clearly that all binaries without exception are already in the third phase of the merging process. This can also be seen in Fig. 11 where we plotted column (8) vs. (10). Only if we use the lower limit for the mass of BL Lac the separation of the BHs is larger by a factor of 1.6 than a_g and consequently the remaining merging time due to emission of gravitational waves exceeds a Hubble time (columns (8) and (10)). Taking the mass from column (7), which is obtained from the $M_{\text{BH}} - \sigma$ relation and therefore might be more reliable, also this source is well beyond the limit to the third phase. For the intermediate masses, $\log(M_{\text{BH}}/M_\odot) = 7.7$ and 7.3 , we obtain $a/a_g = 0.46$ and 0.68 , respectively. As said before a larger mass ratio would further diminish the current separation of the BHs. Thus, even for the lower limit of the mass of BL Lac an equal mass binary would be in the third phase. The smaller the mass ratio is, the larger is the current separation and the longer it takes for the BHs to merge. From column (9), showing the negative logarithm of the mass ratio for which the separation is $a = a_g$ and the remaining merging time is the Hubble time, we see that even for very small mass ratios the binary just enters the third phase. All upper limits are

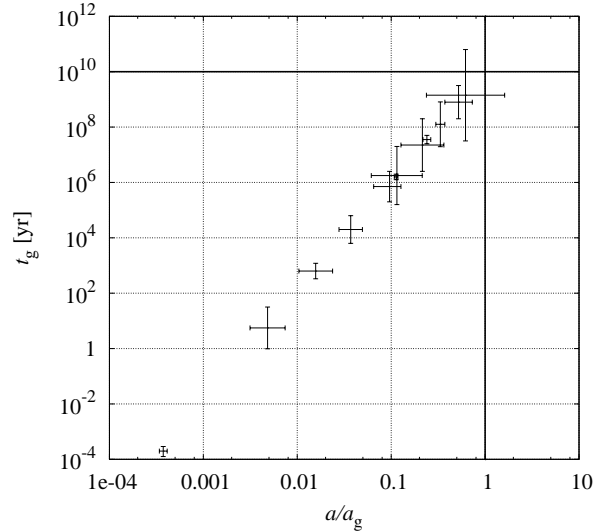


Figure 11. Plot of column (8) vs. (10) of Table 1 for $q = 0.1$. Data lie on the curve defined by Eq. (76) with the errorbars corresponding to the mass ranges in column (4) to (7). Horizontal and vertical lines indicate transition between phases 2 and 3.

smaller than 0.1. Of course BL Lac again is the sole exception, but only for the lower mass limit. All binaries, with the exception of BL Lac for the small mass limit, will coalesce in much less than a Hubble time (column (10)). Using $q = 1$ instead of 0.1 the merging times are smaller by a factor of 0.12 so that the binary in BL Lac will merge in less than a Hubble time also for the small mass limit. In case of eccentric orbits of the BHs the merging times would be further decreased. Thus the times we obtained are actually upper limits. Explaining the variations in the lightcurves with the model by Katz (1997) would result in much smaller periods of the binaries and hence in smaller separations and merging times (Eqs. (76, 79)). Consequently the binary would be even deeper in the third and last phase of the merger. Therefore, provided that the variations in the lightcurves are due to a BHB in the center of the galaxies, our findings in this Section are in very good agreement with the results of the previous Sections and strongly support our conclusions in Paper I: Most likely the slingshot mechanism in the second phase of the merger is sufficiently efficient in order to extract enough energy and angular momentum from the binary so that the BHs can enter the final phase. Hence the profile of the cusp at the beginning of the second phase is very steep indeed, and the binary covers this phase in less than $\sim 10^9$ yr (Section 5.2). Once gravitational radiation dominates the shrinking in the final phase the BHs merge in less than a Hubble time. It is actually striking that all possible non-merged BHBs are observed in all phases but the second, which according to loss-cone depletion models is the one in which binaries should most likely be found.

9 DISCUSSION AND CONCLUSIONS

Observational evidence suggests that BHBs, formed in a galaxy collision, eventually coalesce within less than a Hub-

ble time. Focusing on stars bound to the binary we showed in Paper I that slingshot ejection of stars in the second phase of a merger, which is considered to be the bottleneck, is sufficiently efficient to allow the BHs to coalesce. The prerequisite is a steep cusp which is about as massive as the binary when the binary becomes hard. In this paper, we further pursued this idea and compared its predictions with observations and numerical simulations. Our results verify and strengthen our conclusion of a steep cusp and that the BHs coalesce in less than a Hubble time.

In Sections 3 and 4, we examined in detail the assumptions on which our results in Paper I are based: The kick-parameter is about 1 and we can neglect the cluster potential when calculating the energy which the binary loses to the ejected stars. Our crude theoretical estimate for k is in agreement with the kick-parameter we derived from the data obtained from simulating a stellar cluster in the potential of a binary moving on fixed orbits (Zier 2000). Comparing these values with those obtained in other simulations and scattering experiments (Hills & Fullerton 1980; Roos 1981; Quinlan 1996; Yu 2002) we found very good agreement, justifying our assumption of $k \approx 1$. While including the cluster potential tends to slightly increase the kick-parameter on average, we found that it can be neglected in comparison with the potential of the binary when computing the energy of the stars. The influence of the cusp on the total potential becomes even less for steeper profiles which are required for a successful merger. Hence the assumptions are well justified and we can be confident in our results.

In Section 5, we derived a density profile which enables the BHs to merge and is in agreement with the observed post-merger profiles. Using a deprojected Sérsic model without a cusp for non-core galaxies results in a large amount of total mass for a successful merger if we use a shape parameter $n \approx 5$, which has been found by Trujillo et al. (2004) for the best fits (cf. model (a) in Fig. 4). If, however, a steep central cusp is formed which is removed subsequently by the binary in the second phase, like in model (b), the total mass is much less. To obtain the initial profile, we add such a cusp to a post-merger profile of a core galaxy, best approximated by a core-Sérsic model with $n \approx 5$ (Trujillo et al.). For $\gamma \gtrsim 2.5$ this pre-merger profile allows the BHs to merge without the total mass becoming too large ($\sim 10^{12} M_\odot$), with a core galaxy as merger remnant, see Fig. 6. Without this cusp, i.e. for a flat core with $\gamma \lesssim 2$, either a very large amount of mass is needed, or the binary stalls before it is able to enter the third phase. This is in good agreement with the results from numerical three-body experiments obtained by Roos (1981). Hence we argue that a large and shallow stellar cluster is the end product of a merger while at the time the binary becomes hard a steep cusp is formed which allows the BHs to coalesce. The mass distribution of a core galaxy with a cusp is shown in Fig. 5 by the thin dash-dotted line. It follows a flat power law between a_h and the break radius $r_b \approx 10 a_h$. If core galaxies are merger remnants and the core is formed by mass ejection of the binary we would expect a_h to coincide with r_b . This discrepancy might be caused by the assumption of a too small a_h : Stars bound very tightly to their host BH might increase its effective mass and hence the second phase might start earlier at larger distances. Furthermore we only considered circular stellar orbits. Stars moving on eccentric orbits with apocen-

ters in the range $a_h \lesssim r_+ \lesssim r_b$ and pericenters $r_- \lesssim a_h$ also interact with the binary. The ejection of this additional mass will shift a_h to larger radii, up to r_b for $\epsilon \approx (r_b - a_h)/(r_b + a_h)$. Such stars do not extract as much energy as the more tightly bound stars moving on circular orbits and more mass has to be ejected. However, these stars could compensate for this mass and enable successful mergers in shallower cusps.

Depending on how closely the profile of the ejected mass approaches the initial distribution all slopes for the final profile which are less than that of the cusp are possible. This even includes distributions where the density drops with decreasing radius, which have actually been observed by Lauer et al. (2002). They might indicate that the binary got stalled (Zier & Biermann 2001), but can also be formed by BHs which successfully merge. The maximum of these distributions is observed to be at radii about a factor of 10 larger than a_h , i.e. close to r_b of core galaxies, and thus supports the arguments above for a larger a_h .

At the end of Section 5 we computed the relaxation time of the cusp in dependency of its slope and obtained a couple of 10^8 yr if $\gamma = 3$. For longer times the steep profile is not conserved and if the binary could only eject those stars whose orbital radius is the same as the current semimajor axis, as we assumed to derive Eq. (39), the merger would stall. Of course the BHs, once they have become hard, will influence all stars at $r \lesssim a$, and only if they are very deeply bound in the potential of one of the BHs they will not be ejected. Hence deviations from $\rho \propto r^{-3}$ will not immediately cause the binary to stall. Deriving Eq. (39) we assumed the stars to move on circular orbits. As we pointed out above the inclusion of eccentric orbits allows for shallower ejected profiles ($\gamma \lesssim 3$) which might extend to r_b instead of a_h . The shallower cusps would have a larger relaxation time, see Fig. 9. Thus we expect its lifetime between 10^8 and 10^9 yr for $3 \gtrsim \gamma \gtrsim 2.5$ and the BHs to decay from a_h to a_g on the time scale t_{hg} which is similar or less.

All observational evidence for successfully merged BHs, cited in the introduction, also supports our prediction of the transient formation of a steep cusp. But how is such a cusp formed? Adding adiabatically growing BHs to nonrotating spherical galaxy models and seeking for equilibrium solutions for the cusp, Quinlan et al. (1995) find slopes as steep as 2.5 with an initial $\gamma = 2$ and argue that steeper cusps without central BHs are unlikely. However, the steep cusp which is required for the merger is a transient feature and does not need to be in a state of equilibrium. Indeed, Fig. 3 in Milosavljević & Merritt (2001) suggests that immediately after the merger of both cores when the binary becomes hard the density profile inside a_h is substantially steeper than $\gamma = 2$. Whether this is a real physical effect or due to spurious numerical relaxation still needs to be clarified. When both galaxies merge energy will be dissipated and fractions of angular momentum cancel each other. The amount of these fractions will depend on the initial mass and velocity distributions in the isolated galaxies and on the magnitude and orientation of both galactic spins and the orbital angular momentum relative to each other. The mass that is funneled into the common center of the galaxies will merge with the cores surrounding each BH. At this time the central potential is strongly nonspherical so that both cores will be heavily perturbed, being far from a state of equilibrium, with profiles that might be steeper than $\gamma = 2$.

At $a = a_h$ we expect them to merge into the required steep cusp with a mass of $\sim M_{12}$. At this stage of the merger we can only speculate about the central mass distribution which might be traced with the help of detailed numerical simulations taking into account the above mentioned initial conditions. They will also influence the morphology of the merger product (Toomre & Toomre 1972) as well as processes like the star formation rate and hence the final gas and star content. After the coalescence of the BHs the velocity of the surrounding stars will be tangentially anisotropic at $r \lesssim a_h$ and radially anisotropic at larger radii, with the ejected stars being focused to the equatorial plane of the binary, the more the larger their kinetic energy is (Zier & Biermann 2001). However, if the central regions of the cusp undergo a core collapse before the BHs could merge, possibly leading to the formation of a third BH, this mass is still available for slingshot ejection by the BHs which therefore still can enter the final phase. Our derivation of the initial profile might be oversimplified. A fraction of the ejected stars will stay bound to the cluster at larger distances while the stars remaining in the cusp region are less tightly bound due to the smaller mass in the center and hence will also expand to larger regions. This is enhanced by the energy transfer from the binary to these stars, which are still bound by the BHs, i.e. the heating of this population. Hence, there is a shift of mass within the cluster from the inner to the outer regions, resulting in a profile which is flatter than the difference between the initial and ejected mass distribution. However, the mass deficiency which has been derived by Graham (2004) from the difference between the core-Sérsic fit and the extrapolation of the pure Sérsic profile into the central region amounts to $1-2 M_{12}$. This is in very good agreement with our results, provided that $\gamma \gtrsim 2.5$, see Fig. 7.

Although our approach to the merging of the BHs does not allow to determine the time dependency, we made use of the finding in numerical experiments that the hardening rate is constant once the binary has become hard (Hills 1983; Quinlan 1996; Milosavljević & Merritt 2001; Zier & Biermann 2001), see Section 6. Utilizing this assumption we obtained the semimajor axis and the ejected mass as functions of time with the parameter t_{hg} , the time to decay from a_h to a_g . This is less than 10^9 yr as we concluded from the relaxation time of the cusp in Section 5.4. The exact value of this shrinking time will depend on the mass and velocity distribution of the stars and hence on the initial conditions of the merger. Our results showed that the binary evolves fastest in the beginning of phase 2 and then continuously slows down. Therefore, we conclude that if stalled binaries exist at all, they will most likely be found with a semimajor axis in the range $a_g \lesssim a \lesssim 0.2 a_h$. This is in agreement with the results of numerical three-body experiments by Roos (1981) who finds that a binary might stall at $a \approx 0.015 r_{\text{cusp}}$.

In Section 7, we performed a simple consistency check. In agreement with numerical simulations (Quinlan 1996; Quinlan & Hernquist 1997; Milosavljević & Merritt 2001; Zier & Biermann 2001) we find that the ejected mass is increasing with the number N of mergers if we keep the total mass which merges with m_1 constant. This means that more mass is ejected in N mergers of m_1 with $m_2 = m_1/N$ than in one merger with $m_2 = m_1$. The stronger dependency on N which has been found in the simulations might be due to our

assumption that we can neglect the dependency of the ratio a_h/a_g on the mass ratio q . Our results show that the growth of m_1 during the N mergers has a negligible influence on the total ejected mass.

Ongoing mergers have been observed directly by Komossa et al. (2003) in NGC 6240 with a projected separation of 1.4 kpc, and by Rodriguez et al. (2006) in the elliptical galaxy 0402+379 with a projected separation of both nuclei of only 7.3 pc. Thus both mergers are still in the first phase and are clearly far from being stalled at the end of the second phase in a distance of a few 0.01 pc. Other promising sources with still existing binaries could be pure Z-shaped radio galaxies (Gopal-Krishna, et al. 2003) with a separation less than 30-100 kpc (Zier 2005). Such objects might have been observed for the first time in a new sample of about 100 XRG candidates, see Cheung (2007). Possibly some of these sources exhibit broad-emission lines characteristic of quasars (Cheung, priv. comm.) as have been observed only recently in some XRGs (Wang et al. 2003; Landt et al. 2006). This actually strengthens the conjecture that merging BHBs are the formation mechanism for XRGs and the central torus in AGN (Zier & Biermann 2001, 2002), which is required by the unification scheme for type 1 and 2 AGN (Antonucci 1993): The symmetry axis of the torus, which is surrounding the nucleus and the broad emission line region (BLR), is aligned with the post-merger jet. Because in XRGs both lobes are close to the plane of sky we consequently see the torus almost edge on with the BLR hidden in its center. This is in good agreement with so few XRGs exhibiting BLRs. The larger the angle between the plane of sky and the post-merger jet, i.e. the axis of the torus, the more from within the torus we can see, including the BLR, and the less reddened the core should appear. For such objects we predict shorter post-merger jets in projection. According to the merging scenario XRGs are seen close to edge-on and hence they should be good candidates for showing a type 1 spectrum in polarized light like NGC 1068 (Antonucci & Miller 1985).

Stalled binaries are expected at the end of the second phase when slingshot ejection of stars becomes inefficient according to some interpretations of numerical simulations. In Section 8, we tested this prediction and made use of a compilation of 12 sources (Merritt & Milosavljević 2005) which exhibit periodic variations in their lightcurves. These might be caused by the orbital motion of a BHB. From the observed periods and masses obtained with various methods we determined the current semimajor axis of the binary, assuming a mass ratio $q = 0.1$. We find that all binaries have already shrunk deep into the third phase and that the remaining time to coalescence in all sources is much less than a Hubble time. The remaining merging time increases with decreasing mass ratio and therefore we computed q for the case that it still needs a Hubble time to merge. We obtained values much smaller than $q = 0.1$ and hence even in case of minor mergers the binary is already in the third phase. Some of the mass estimates differed by large factors, in case of BL Lac by 100. The smallest mass obtained with the method of minimal time scales (Xie et al. 2002) gives the only source that is still in the second phase if $q < 0.98$. However, for a larger mass which has been obtained with the probably more reliable $M_{\text{BH}} - \sigma$ relation (Gebhardt et al. 2000; Tremaine et al. 2002) also this binary is clearly beyond the

transition to the final phase. Thus, in striking contrast to the predictions of loss-cone depletion (e.g. Begelman et al. 1980; Quinlan 1996; Makino 1997; Quinlan & Hernquist 1997; Milosavljević & Merritt 2001; Berczik et al. 2005) we find all BHB candidates to be already in the phase where the emission of gravitational waves dominates the decay. Therefore a merger with a third galaxy before the BHs have coalesced and the formation of three bound supermassive BHs with the subsequent slingshot ejection of one or more BHs (e.g. Valtonen 1996) is highly unlikely.

We conclude that the BHB which forms in a galaxy collision merges completely. This is in agreement with the observation of mostly merged binaries and only few ongoing mergers with none of them being stalled in the second phase. Hence the slingshot ejection of stars is sufficiently effective arguing for the formation of a steep cusp at the time when the binary becomes hard and which contains a mass of $\sim M_{12}$, as we derived it in Paper I and the present article. Triaxial potentials where the loss-cone is always full (Yu 2002; Holley-Bockelmann et al. 2002; Holley-Bockelmann & Sigurdsson 2006; Berczik et al. 2006) further support our arguments for a successfully merged binary. The inclusion of dark matter into our analysis, which we did not consider here although the same formalism applies, would accelerate the merger and make it even more likely that the BHs coalesce. If there is not enough baryonic matter in the cusp to allow the BHs to merge but they have coalesced anyway, our approach should provide a tool to draw conclusions about the amount and distribution of dark matter in the cusp region. However, we may conclude that stalled binaries do not exist at all or are very rare.

ACKNOWLEDGMENTS

I would like to thank Wolfram Krüßs for his valuable comments to improve this manuscript. I am also grateful to the anonymous referee for helpful advice and comments. It is a pleasure to acknowledge the generous support and hospitality I experienced at the Raman Research Institute. I also wish to acknowledge the hospitality of Peter Biermann and his group at the Max-Planck Institute for Radioastronomy while finishing the work on this paper.

REFERENCES

- Abramowitz M., Stegun I. A., 1972, *Handbook of Mathematical Functions*. Handbook of Mathematical Functions, New York: Dover, 1972
- Antonucci R., 1993, *ARA&A*, 31, 473
- Antonucci R. R. J., Miller J. S., 1985, *ApJ*, 297, 621
- Barnes J. E., Hernquist L., 1996, *ApJ*, 471, 115
- Begelman M. C., Blandford R. D., Rees M. J., 1980, *Nat.*, 287, 307
- Berczik P., Merritt D., Spurzem R., 2005, *ApJ*, 633, 680, astro-ph/0507260
- Berczik P., Merritt D., Spurzem R., Bischof H.-P., 2006, *ApJ*, 642, L21, astro-ph/0601698
- Binney J., Tremaine S., 1994, *Galactic Dynamics*. Princeton Series in Astrophysics
- Carollo C. M., Franx M., Illingworth G. D., Forbes D. A., 1997, *ApJ*, 481, 710, astro-ph/9701218
- Cheung C. C., 2007, *AJ*, 133, 2097, astro-ph/0701278
- Dennett-Thorpe J., Scheuer P. A. G., Laing R. A., Bridle A. H., Pooley G. G., Reich W., 2002, *MNRAS*, 330, 609, astro-ph/0110339
- Dermer C. D., Gehrels N., 1995, *ApJ*, 447, 103
- Fan J. H., Xie G. Z., Lin R. G., Qin Y. P., Li K. H., Zhang X., 1997, *A&AS*, 125, 525
- Fan J. H., Xie G. Z., Pecontal E., Pecontal A., Copin Y., 1998, *ApJ*, 507, 173, astro-ph/9809050
- Gebhardt K., Bender R., Bower G., Dressler A., Faber S. M., Filippenko A. V., Green R., Grillmair C., Ho L. C., Kormendy J., Lauer T. R., Magorrian J., Pinkney J., Richstone D., Tremaine S., 2000, *ApJ*, 539, L13, astro-ph/0006289
- Gebhardt K., Richstone D., Ajhar E. A., Lauer T. R., Byun Y.-I., Kormendy J., Dressler A., Faber S. M., Grillmair C., Tremaine S., 1996, *AJ*, 112, 105, astro-ph/9604092
- Gergely L. Á., Biermann P. L., 2007, *ArXiv e-prints*, 704, 0704.1968
- Ghez A. M., Duchêne G., Matthews K., Hornstein S. D., Tanner A., Larkin J., Morris M., Becklin E. E., Salim S., Kremenek T., Thompson D., Soifer B. T., Neugebauer G., McLean I., 2003, *ApJ*, 586, L127, astro-ph/0302299
- Gopal-Krishna, Biermann P. L., Wiita P. J., 2003, *ApJ*, 594, L103, astro-ph/0308059
- Gopal-Krishna, Wiita P. J., Joshi S., 2007, *MNRAS submitted*
- Graham A. W., 2004, *ApJ*, 613, L33, astro-ph/0503177
- Graham A. W., Erwin P., Trujillo I., Asensio Ramos A., 2003, *AJ*, 125, 2951, astro-ph/0306023
- Haehnelt M. G., Kauffmann G., 2002, *MNRAS*, 336, L61, astro-ph/0208215
- Hayashida N., Hirasawa H., Ishikawa F., Lafoux H., Nagano M., Nishikawa D., Ouchi T., Ohoka H., Ohnishi M., Sakaki N., Sasaki M., Shimodaira H., Teshima M., et al. 1998, *ApJ*, 504, L71+
- Hills J. G., 1983, *AJ*, 88, 1269
- Hills J. G., Fullerton L. W., 1980, *AJ*, 85, 1281
- Holley-Bockelmann K., Mihos J. C., Sigurdsson S., Hernquist L., Norman C., 2002, *ApJ*, 567, 817, astro-ph/0111029
- Holley-Bockelmann K., Sigurdsson S., 2006, *ArXiv Astrophysics e-prints*, astro-ph/0601520
- Kaspi S., Smith P. S., Netzer H., Maoz D., Jannuzi B. T., Giveon U., 2000, *ApJ*, 533, 631, astro-ph/9911476
- Katz J. I., 1997, *ApJ*, 478, 527
- Komossa S., 2003, in Centrella J. M., ed., *The Astrophysics of Gravitational Wave Sources Vol. 686 of American Institute of Physics Conference Series*, Observational evidence for supermassive black hole binaries. pp 161–174, astro-ph/0306439
- Komossa S., 2006, *Memorie della Societa Astronomica Italiana*, 77, 733
- Komossa S., Burwitz V., Hasinger G., Predehl P., Kaastra J. S., Ikebe Y., 2003, *ApJ*, 582, L15, astro-ph/0212099
- Lainela M., Takalo L. O., Sillanpää A., Pursimo T., Nilsson K., Katajainen S., Tosti G., Fiorucci M., Luciani M., Villata M., Raiteri C. M., et al. 1999, *ApJ*, 521, 561
- Landt H., Perlman E. S., Padovani P., 2006, *ApJ*, 637, 183, astro-ph/0509718

- Lauer T. R., Ajhar E. A., Byun Y.-I., Dressler A., Faber S. M., Grillmair C., Kormendy J., Richstone D., Tremaine S., 1995, *AJ*, 110, 2622
- Lauer T. R., Gebhardt K., Richstone D., Tremaine S., Bender R., Bower G., Dressler A., Faber S. M., Filippenko A. V., Green R., Grillmair C. J., Ho L. C., Kormendy J., Magorrian J., Pinkney J., Laine S., Postman M., van der Marel R. P., 2002, *AJ*, 124, 1975, astro-ph/0206122
- Lima Neto G. B., Gerbal D., Márquez I., 1999, *MNRAS*, 309, 481, astro-ph/9905048
- Liu F. K., Liu B. F., Xie G. Z., 1997, *A&AS*, 123, 569, astro-ph/9610208
- Liu F. K., Wu X.-B., Cao S. L., 2003, *MNRAS*, 340, 411, astro-ph/0310045
- Liu F. K., Xie G. Z., Bai J. M., 1995, *A&A*, 295, 1
- Makino J., 1997, *ApJ*, 478, 58, astro-ph/9608161
- Márquez I., Lima Neto G. B., Capelato H., Durret F., Gerbal D., 2000, *A&A*, 353, 873, astro-ph/9911464
- McLure R. J., Dunlop J. S., 2001, *MNRAS*, 327, 199, astro-ph/0009406
- Merritt D., Graham A. W., Moore B., Diemand J., Terzić B., 2006, *AJ*, 132, 2685, astro-ph/0509417
- Merritt D., Milosavljević M., 2005, *Living Reviews in Relativity*, 8, 8, astro-ph/0410364
- Milosavljević M., Merritt D., 2001, *ApJ*, 563, 34, astro-ph/0103350
- Peters P. C., 1964, *Phys. Rev. B*, 136, 1224
- Prugniel P., Simien F., 1997, *A&A*, 321, 111
- Pursimo T., Takalo L. O., Sillanpää A., Kidger M., Lehto H. J., Heidt J., Charles P. A., Aller H., Aller M., Beckmann V., Benítez E., Bock H., et al. 2000, *A&AS*, 146, 141
- Quinlan G. D., 1996, *New Astronomy*, 1, 35, astro-ph/9601092
- Quinlan G. D., Hernquist L., 1997, *New Astronomy*, 2, 533, astro-ph/9706298
- Quinlan G. D., Hernquist L., Sigurdsson S., 1995, *ApJ*, 440, 554+
- Raiteri C. M., Villata M., Aller H. D., Aller M. F., Heidt J., Kurtanidze O. M., Lanteri L., Maesano M., Massaro E., Montagni F., Nesci R., Nilsson K., et al. 2001, *A&A*, 377, 396, arXiv:astro-ph/0108165
- Rauch K. P., Tremaine S., 1996, *New Astronomy*, 1, 149, astro-ph/9603018
- Ravindranath S., Ho L. C., Peng C. Y., Filippenko A. V., Sargent W. L. W., 2001, *AJ*, 122, 653, astro-ph/0105390
- Rest A., van den Bosch F. C., Jaffe W., Tran H., Tsvetanov Z., Ford H. C., Davies J., Schafer J., 2001, *AJ*, 121, 2431, astro-ph/0102286
- Rodriguez C., Taylor G. B., Zavala R. T., Peck A. B., Pollack L. K., Romani R. W., 2006, *ApJ*, 646, 49, astro-ph/0604042
- Roos N., 1981, *A&A*, 104, 218
- Rottmann H., 2001, PhD thesis, University of Bonn, http://hss.ulb.uni-bonn.de/diss_online/math_nat_fak/2001/rottmann_helge/0074.pdf
- Saslaw W. C., Valtonen M. J., Aarseth S. J., 1974, *ApJ*, 190, 253
- Schödel R., Ott T., Genzel R., Eckart A., Mouawad N., Alexander T., 2003, *ApJ*, 596, 1015, astro-ph/0306214
- Schoenmakers A. P., de Bruyn A. G., Röttgering H. J. A., van der Laan H., Kaiser C. R., 2000, *MNRAS*, 315, 371, astro-ph/9912141
- Sillanpää A., Haarala S., Valtonen M. J., Sundelius B., Byrd G. G., 1988, *ApJ*, 325, 628
- Terzić B., Graham A. W., 2005, *MNRAS*, 362, 197, astro-ph/0506192
- Toomre A., Toomre J., 1972, *ApJ*, 178, 623
- Tremaine S., Gebhardt K., Bender R., Bower G., Dressler A., Faber S. M., Filippenko A. V., Green R., Grillmair C., Ho L. C., Kormendy J., Lauer T. R., Magorrian J., Pinkney J., Richstone D., 2002, *ApJ*, 574, 740, astro-ph/0203468
- Trujillo I., Erwin P., Asensio Ramos A., Graham A. W., 2004, *AJ*, 127, 1917, astro-ph/0403659
- Valtaoja E., Teräsanta H., Tornikoski M., Sillanpää A., Aller M. F., Aller H. D., Hughes P. A., 2000, *ApJ*, 531, 744
- Valtonen M. J., 1996, *MNRAS*, 278, 186
- Wang J.-M., Luo B., Ho L. C., 2004, *ApJ*, 615, L9, astro-ph/0412074
- Wang T.-G., Zhou H.-Y., Dong X.-B., 2003, *AJ*, 126, 113
- Xie G. Z., Li K. H., Zhang X., Bai J. M., Liu W. W., 1999, *ApJ*, 522, 846
- Xie G. Z., Liang E. W., Xie Z. H., Dai B. Z., 2002, *AJ*, 123, 2352
- Xie G. Z., Liang E. W., Zhou S. B., Li K. H., Dai B. Z., Ma L., 2002, *MNRAS*, 334, 459
- Xie G. Z., Zhou S. B., Liang E. W., 2004, *AJ*, 127, 53
- Yu Q., 2002, *MNRAS*, 331, 935, astro-ph/0109530
- Zhang X., Xie G. Z., Bai J. M., 1998, *A&A*, 330, 469
- Zhao J.-H., Bower G. C., Goss W. M., 2001, *ApJ*, 547, L29, astro-ph/0011169
- Zier C., 2000, PhD thesis, University of Bonn
- Zier C., 2005, *MNRAS*, 364, 583, astro-ph/0507129
- Zier C., 2006, *MNRAS*, 371, L36, astro-ph/0605619
- Zier C., Biermann P. L., 2001, *A&A*, 377, 23, astro-ph/0106419
- Zier C., Biermann P. L., 2002, *A&A*, 396, 91, astro-ph/0203359